Study for the effect of cyanoacrylate based nanoparticles on freshwater unicellular algae

by

Dwiyantari Widyaningrum
Student ID Number: 1188002

A dissertation submitted to the
Engineering Course, Department of Engineering,
Graduate School of Engineering,
Kochi University of Technology,
Kochi, Japan

in partial fulfillment of the requirements for the degree of
Doctor of Engineering

Assessment Committee:
Supervisor : Takeshi Ohama
Co-Supervisor : Sakae Horisawa
Co-Supervisor : Osamu Ariga
Yusuke Kamachi
Seiji Tanaka
Masayuki Ike

March 2018

ABSTRACT

Nanoparticles have unique properties that make them attractive for use in industrial and medical technology industries but can also be harmful to living organisms, making an understanding of their molecular mechanisms of action essential. We examined the effect of three different sized acrylic resin nanoparticles (acrNPs) on the unicellular green alga *Chlamydomonas reinhardtii.* We found that exposure to acrNPs immediately caused *C. reinhardtii* to display abnormal swimming behaviors. Furthermore, after one hour, most of the cells had stopped swimming, and 10–30% of cells were stained with trypan blue, suggesting that these cells had severely impaired plasma membranes. Observation of the cyto-ultrastructure showed that the cell walls had been severely damaged and that many acrNPs were located in the space between the cell wall and plasma membrane, as well as inside the cytosol in some cases. A comparison of three strains of *C. reinhardtii* with different cell wall conditions further showed that the cell mortality ratio increased more rapidly in the absence of a cell wall. Interestingly, cell mortality over time was essentially identical regardless of acrNP size if the total surface area was the same. Cell mortality was accompanied by the overproduction of reactive oxygen species, which was detected more readily in cells grown under constant light rather than in the dark. Moreover, by exposure with acrNPs at a very high concentration (1 g/L), around 60 % of the *Chlorella vulgaris* cells were changed into protoplasts or spheroplasts (protoplasts/spheroplasts), without the induction of cell mortality. At the same concentrations (w/v) of acrNPs, smaller particles worked much more efficiently than larger ones to induce mortality, or to generate protoplasts/spheroplasts. Filtrate prepared from the medium of *C. vulgaris*

exposure with acrNPs contained evidence of cell wall lytic activity. Furthermore, direct observation of the trails of acrNPs indicated that the first trigger was their contact with the cell wall, which is most likely accompanied by the inactivation or deprivation of proteins on the cell wall surface that seemed to stimulate the secretion of cell-wall hydrolytic enzyme(s) and the further abnormalities in the cells.

Keywords: acrylic resin nanoparticles, *Chlamydomonas*, *Chlorella*, cell mortality, protoplast

TABLES OF CONTENTS

LIST OF FIGURES

LIST OF TABLES

CHAPTER 1. General Introduction

Nanotechnology is an emerging technology and has a potential to produce a lot of variety of new material with unique physicochemical characteristic in nanoparticle size. Nanomaterials have been used in various industrial sectors (e.g., construction, electronics, food, consumer goods, medical, et al.). Nanoparticle (NP) is a particle with size in at least one dimension falling into the nanoscale or less than 100 nm [1-2]. Engineered nanoparticles (ENPs) is used to refer a nanoparticle that intentionally designed and produced. Therefore, the ENPs have a narrow distribution of size [3].

ENPs are grouped depending on their chemical composition such as (1) carbon NPs (e.g., carbon nanotubes and fullerenes), (2) metal oxide NPs (e.g., ZnO NPs and TiO2 NPs), (3) metal NPs (e.g., Au-NPs and Ag-NPs), (4) semiconductor NPs (e.g., Quantum dots), and (5) polymeric nanomaterials [4]. Polymeric NPs are made from the natural polymers (e.g., chitosan, alginate, and albumin), the non-biodegradable polymers (e.g., polyacrylamide, polystyrene, and polyacrylates), and the biodegradable polymers (e.g., polylactic acid, poly alkyl cyanoacrylate, and poly amino acid). Polymeric NPs are biocompatible and have a non-toxic characteristic which made this NPs widely applied in medical technology for drug delivery, wound healing, and antibacterial material [5-6].

ENPs have substantially differed properties from those bulk material of the same composition that attributable to their small size, chemical composition, surface structure, solubility, shape, and aggregation. The particle size and surface of ENPs are the important determinants for its reactivity, transport, and toxicity. As the size of a particle decreases, its surface area increases and creates the opportunity to strongly interact with biological tissues and organic material in the environment. The unique

properties of ENPs make them not only attractive for industrial and medical technology but also possibly harmful to living organism and environment. Furthermore, ENPs potentially could generate toxicity [1-3,7-8].

In the aquatic environment, NPs undergo important structural transformations as well as changes in structure, shape, and size due to aggregation, solubilization or adsorption phenomena which could affect their reactivity, toxicity, and behavior [9]. The surface properties of NPs (e.g., ionic strength, PH, particle concentration, and size, etc.) are the key factors to determine the stability of NPs as the colloidal suspension for aggregation and deposition in the aquatic system [1]. Moreover, the composition of natural organic matter (NOM) in the aquatic environment also determines the NPs aggregation and deposition. NPs, because of its surface properties, interact with NOM and form large aggregates that will further increase the complexity and could affect the behavior of NPs in the aquatic environment [10]. The experiment with aquatic organisms has demonstrated that the presence of NPs in media leads to decreased fertility, physiological changes, behavior abnormalities, and an increased mortality rate [4].

In this dissertation, we reported about the effect of polymeric nanoparticles that was composed by isobutyl cyanoacrylate on unicellular algae. Unexpectedly we found that isobutyl-cyanoacrylate based nanoparticles (hereafter acrNPs) could induce cell mortality and physiological abnormalities in unicellular algae which the effects of coincubation of acrNPs were different based on algae species. We also described the possible mechanisms for these actions.

In the general introduction chapter, we provided overviews about (1) the application of cyanoacrylate in medical technology especially for the antibacterial agent

and (2) the interaction between ENPs such as metal oxide NPs, carbon nanotubes, and PSNPs with unicellular algae.

1.1 Cyanoacrylate and its application in medical technology

1.1.1 Cyanoacrylate application as tissue adhesives

Cyanoacrylate, an acrylic resin, is well known as quick and strong adhesives with industrial, household, and medical uses. It is known that methyl, ethyl, butyl, and octyl cyanoacrylates are commonly used as bases for commercial cyanoacrylate adhesives [11]. The monomers of cyanoacrylate rapidly polymerize in the presence of water to form long and strong chains in the process namely anionic and zwitterionic polymerization. Previous studies had been done since the early 1960s to investigate the possible use of several cyanoacrylates in the medical field, for example as tissue adhesives [11-13].

Studies showed that short alkyl chain cyanoacrylates (e.g., methyl and ethyl cyanoacrylate) are toxic to animal tissue. The rapid degradation of short alkyl chain cyanoacrylates implies a high concentration of cyanoacetate and formaldehyde as degradation products leading to chronic inflammation in cells [14-15]. Butyl cyanoacrylate (BCA) and Octyl cyanoacrylate (OCA) are not toxic when applied topically. The slow degradation of longer alkyl chain cyanoacrylates implies a limited accumulation of by-product that can be quickly eliminated by tissues [14].

Cyanoacrylate tissue adhesives are widely used in the surgeries (e.g., plastic surgery, repairing incisions and, affixing skin graft) because of several advantages such as rapid closure time, simple and painless application, non-toxic, and no requirement for removal [12,16]. n-butyl cyanoacrylate (NBCA), the medium-length alkyl chain, based skin adhesives have 15 times faster closure duration than that of surgical suture which

could decrease the surgery time. The patients also benefit from the convenience of avoiding post-operative suture removal, which is practical for those coming from long distances, and those who are poorly mobile [15]. OCA, the long alkyl chain, also have rapid closure time. Study of 814 patients with skin lesion and scar revision showed that OCA closure was less painful and significantly less time than that of standard suture [14].

Some studies also reported that cyanoacrylate based skin adhesives (e.g., Histoacryl® and Dermabond®) have antibacterial properties both in vitro and in vivo [16]. The polymerization reaction appears to have an essential contributory role in the antibacterial activity of cyanoacrylate tissue adhesives [17]. The cyanoacrylate-based tissue adhesives showed no effect on Gram-negative bacteria, and there was significant bacteriostatic activity against Gram-positive bacteria. The presence of lipopolysaccharide capsule surrounding the cell wall of the Gram-negative microbes may act as a barrier to the glue and explain the glue's ineffectiveness for the organism [18].

1.1.2 Cyanoacrylate application for drug delivery agents and coating material

Polymeric NPs have emerged as promising drug carriers because of their advantages such as easy fabrication and functionalization, biocompatibility, sustained drug release, and controllable degradation rate [19]. Poly alkyl cyanoacrylate (PACA) nanoparticle is one kind of polymeric NPs that recently gains interest to develop as biodegradable drug carriers to tissues, cells, or subcellular compartments. PACA NPs for drug carriers were designed to form a nanosphere or core-shell nanosphere. The preparation of PACA NPs includes the polymerization of different alkyl cyanoacrylate monomers or directly from the polymers [20].

The major interest studies for drug delivery particles are uptake profile, degradation rate, and cytotoxicity moreover the different lengths of alkyl cyanoacrylate influence those characteristics. The cellular uptake mechanism of drug carrier NPs including PACA NPs was predominantly by endocytosis that the efficacy was determined by physicochemical properties of NPs and cell-type dependent [21-23]. In vitro study using PC3 cells and RBE4 cells showed different uptake efficiency between poly octyl cyanoacrylate (POCA) and poly butyl cyanoacrylate (PBCA) nanoparticles. The higher uptake of POCA NPs in PC3 cells also influenced by different zeta potential of NPs which PBCA NPs became more negatively charged than POCA NPs [23].

Many drugs can be entrapped in nanospheres of PACA then released inside the cell due to NP degradation. Intracellular NP degradation results in alkyl alcohol and poly cyanoacrylic acid. The degradation occurs by surface erosion that is catalyzed by esterase. According to this mechanism, nanoparticles are usually degraded within a couple of hours depending on the alkyl side chain length of the PACA forming the nanospheres [22,24-25].

Several studies of PACA incubation on macrophages described that PACA nanospheres cytotoxicity attributed to the presence of degradation products. Gipps et al. [26] showed that the cell viability was influenced dramatically by the nature of the polymer nanospheres that made from PACA with different length of the side chain. Another study by Lherm et al. [21] showed that after incubating PACA nanoparticles with L929 fibroblasts, only nanoparticles with slow degradation kinetics (i.e., long alkyl side chain) were non-toxic. Cytotoxicity of alkyl cyanoacrylate polymers is apparently dependent upon the length of the alkyl side chain, with a very low toxicity for the longer alkyl chain side.

Polymeric nanospheres are a promising material for coating the antibiotic. The coating was aimed to maintain the structure and to decelerate the degradation of antibiotics. Moreover, the modification on the surface of NPs could increase the uptake and specificity of antibiotics into cells, raising the drug's effectiveness [27-28].

In the initial studies, PACA has been used as a material for preparing antibiotic-loaded polymeric NPs for the treatment of several infections caused by different bacteria and have shown enhanced therapeutic efficacy. In vivo studies in experimentally infected C57BL/6 mice reported that the therapeutic index of ampicillin loaded poly iso-hexyl cyanoacrylate (PIHCA) NPs against *Salmonella typhimurium* increased 120-fold compared to that of free ampicillin. The same study also showed that 0.8 mg of ampicillin incorporated into NPs had a more significant therapeutic effect as compared with 48 mg of free ampicillin against *S. typhimurium* [29]. Poly ethyl cyanoacrylate (PECA) NPs containing pefloxacin and ofloxacin quinolone antibiotics showed twofold to 50- fold more antimicrobial activity against *P. aeruginosa, S. aureus, E. coli, and Enterococcus faecalis* [30]. Besides, encapsulation of moxifloxacin within PBCA NPs demonstrated an improvement of antimicrobial activity against *M. tuberculosis* [31]. The enhancement of drug efficacy was determined by rapid uptake of loaded antibiotic NPs by the infected cells or the bacteria cells, with the subsequent intracellular release of the drug [27-31].

Recently, Shirotake [32] reported that *n*-butyl cyanoacrylate (NBCA) NPs without binding with any antibiotic could induce cell lysis in Gram-positive bacteria, such as *Staphylococcus aureus* and *Enterococci* sp., but not in Gram-negative bacteria. Shirotake [32] proposed a hypothesis that NBCA NPs directly attach to the peptidoglycan layer of Gram-positive bacteria, where they locally inhibit peptidoglycan synthesis at the attachment site, finally inducing bacteriolysis by preventing synthesis of

the peptidoglycan layer evenly across the plasma membrane. In Gram-negative bacteria, of which the outermost surface is lipid monolayer, NBCA NPs cannot directly bind to the peptidoglycan layer; therefore, Gram-negative bacteria are not sensitive to NBCA NPs.

1.2 Toxicological effect of Engineered nanoparticles (ENP) on unicellular algae

The broad application of ENPs in industry and consumer used products are progressively releasing them into our aquatic environment. Studies about ENPs toxic effect to marine and freshwater unicellular algae were intensively increased during last few years, as shown by a large number of publications on this subject. ENPs have toxicological effects on unicellular algae such as oxidative stress, cell damage, and reduction in photosynthetic activity [3-4]. Besides, extracellular polymeric substances (EPS) production has been shown to increase in algae upon exposure to ENPs, contributing to detoxification mechanism [33]. The toxic effects of ENPs to aquatic organisms are attributed to the direct effects (e.g., chemical composition and physiochemical properties) and the indirect effects (e.g., the physical restraints, the releasing of toxin, and the production of ROS) [3,7-8,34-36].

Toxicological studies of metal and metal oxide NPs on several marine and freshwater algal species had been reported. The toxic effects of metal and metal oxide NPs were suggested due to NPs adsorption on the algal cell wall, ROS generation, metals ion released from NPs, and simultaneous effects of various factor. Besides, NPs size and surface properties also attribute to the NPs toxicity on algae [35].

Silver (Ag) is one of the most toxic trace elements known to algae. Navarro et al. [36] reported that the exposure of AgNP could reduce the photosynthesis activity in

Chlamydomonas reinhardtii. Ag-NPs are toxic by releasing Ag+ that rapidly uptake probably via copper transporter. Moreover, Ag+ causes photosynthesis inhibition, growth inhibition, and ROS generation [37-38]. In addition, the study in *Ochromonas danica* found the accumulation of Ag-NPs within algal cells, where they were able to exert their toxic effect [39]. The solubility of Ag-NPs partly relates to NPs toxic effects. The aggregation of Ag-ENPs resulted in the rapid release of Ag+ that led to the suppression of cell growth and reduction of photosynthesis activity in *Thalassiosira weissflogii* [33].

Gold nanoparticles (Au-NPs) have been utilized in high technology applications such as electronic conductors, catalysis, sensory probes, therapeutic agent, diagnostics, and drug delivery. Few toxicological studies of Au-NPs differing in coating and size on *Pseudokirchneriella subcapitata* and *Scenedesmus obliquus* showed a moderate toxicity on algal growth and photosynthesis activity with the effective concentration in the mg/L Au-NPs range [40-41]. Study of Au-NPs toxicity effects on *Chlamydomonas reinhardtii* showed that Au-NPs did not give any effects on algal growth and photosynthesis activity [42].

Titanium oxide (TiO2) and Zinc oxide (ZnO) nanoparticles have been widely used in consumer products such as paints, coatings, pharmaceutical, and cosmetics. Longer coincubation time of TiO2-NPs and ZnO-NPs reduced the photosynthesis activity and inhibited the algal growth in *Desmosdesmus subspicatus* and *Pseudokirchneriella subcapitata*. In aquatic environment, the toxic effects of TiO2-NPs are mainly determined by their size and specific surface area. In the study using *Desmodesmus subspicatus* and *Pseudokirchneriella subcapitata*, bulk TiO2 (size >100 nm) were less toxic than the nano-sized TiO2, which the particles size less than 25 nm [43-44]. Nanoparticles have greater surface area per mass, compared with the bulk form of the

same chemistry, serves NPs more reactive biologically [43]. In *Pseudokirchneriella subscapitata*, ZnO-NPs were more toxic than that of bulk material, but the toxicity effect was determined by solubilized Zn2+ ion [44]. Further study found that ZnO-NP solubility, pH, and aggregation influenced the releasing of ZnO2+ ion [45]. Moreover, ZnO-NPs in high concentrations were strongly adsorbed on the cell wall of *Chlorella* sp. that potentially damaged the cells [46].

Carbon nanotubes (CNTs) have been utilized in various applied technology such as agricultural, biomedical, electronics, and mechanical. In the recent years, the production of CNTs has significantly increased and exceed several thousand tons per year. Recently, several studies have reported about toxic effects of CNTs to freshwater and marine algae. CNTs are assumed can induce the generation of ROS that causes oxidative stress to the unicellular algae [47].

CNTs were reported to cause growth inhibition and photosynthesis activity reduction in algae. In *Pseudokirchneriella subcapitata* and *Chlorella vulgaris*, growth inhibition was occurred within the first 72 hours and had a positive correlation with CNTs agglomeration [48-49]. In the study using *Chlamydomonas reinhardtii*, 50% cell mortality ratio reached after long-term exposure with a low concentration of fullerenes [50]. Moreover, the rest of cells had difficulties on cell reproduction and showed a reduction in photosynthesis activity [50-51]. The authors suggested that oxidative stress, as a result of NPs shading and agglomeration, attributed the CNTs toxic effects. Shading is often speculated to explain the reduced viability of phototrophic organisms exposed to nanoparticles [47-51].

Polymer nanoparticles have attracted increased attention over the past several years in a variety of fields including catalysis, coatings, medicine, electronics, and polymeric composites. Polyethylene and polystyrene nanoparticles are the typical types of polymer

nanoparticle that have been used in consumer products especially for personal care products such as cosmetic or facial wash. Nowadays, plastic debris and plastic fragment become one of the major pollutions in the fresh and marine water system that potentially give a dangerous effect on aquatic species.

Several studies reported that polystyrene nanoparticles (PSNPs) gave limited toxic effects on microalgae [52]. Coincubation of PSNPs caused the growth inhibition in *Pseudokirchneriella subcapitata* [53] and the photosynthesis activity reduction in *Chlorella vulgaris* [54]. Exposing of PSNPs to *Euglena gracilis* caused morphological changes of the cell to rounder shape. No toxic effects were observed in *Haematococcus pluvialis* and *Chlamydomonas reinhardtii* after four hr exposure with no charge PSNPs at final concentration 1 mg/mL but the increment of EPS production was found upon the coincubation of PSNPs [55].

The authors suggested that the adsorption of NPs on the algae cell wall and the formation of algae-NPs agglomeration determined the PSNPs toxic effects [53-54]. Similar to CNTs, shading because of NPs adsorption was postulated to affect the photosynthesis activity in algae cells. Adsorption of PSNPs on cell wall but not PSNPs internalization was observed in *Chlorella vulgaris, Pseudokirchneriella subcapitata*, *Euglena gracilis, Haematococcus pluvialis*, and *Chlamydomonas reinhardtii* [52-55].

Physicochemical properties of PSNPs determined the NPs reactivity to algae cell. Adsorption of neutral and positively charged PSNPs on the cell wall of *Pseudokirchneriella subcapitata* was stronger than that of negatively changed PSNPs [53]. Li [55] also reported that adsorption of 50 nm of PSNPs on the cell wall was stronger than that of 500 nm of PSNPs. Therefore, the EPS production was observed in *Haematococcus pluvialis* only when the cells were coincubated with 50 nm size of PSNPs but not with 500 nm size of PSNPs.

1.3 References

1. Maurer-Jones MA, Gunsolus IL, Murphy CJ, and Haynes CL. Toxicity of engineered nanoparticles in the environment. Anal Chem. 2013. 85 (6): 3036-3049.
2. Singh AK. Introduction to nanoparticles and nanotoxicology. In Engineered nanoparticles: structure, properties, and mechanism of toxicity. Academic press. 2016. pp 1-18
3. Navarro E, Baun A, Behra R, Hartmann NB, Filser J, Miao AJ, Quigg A, Santchi PH, and Sigg L. Environmental behavior and ecotoxicity of engineered nanoparticles to algae, plants, and fungi. Ecotoxicology. 2008. 17(5): 372-386.
4. Yu E, Pavlov DS, Demidova TB, and Dgebuadze YY. Effect of nanoparticles on aquatic organisms. Biology Bulletin. 2010. 37(4): 406-412.
5. Banik BL. Fatthani P, and Brown JL. Polymeric nanoparticles: the future of nanomedicine. WIREs nanomedicine and nanotechnology. 2016. 8: 271-299.
6. Bhatia S. Nanoparticles types, classification, characterization, fabrication methods, and drug delivery application. In Natural polymer and delivery system. Switzerland: Springer international publishing. 2016. pp 33-93.
7. Nel A, Xia T, Madler L, and Li N. Toxic potential of materials at the nanolevel. Science. 2006. 311(5761): 622-627.
8. Rana S, and Kalaichelvan PT. Ecotoxicity of nanoparticles. ISRN Toxicology. 2013. Article ID 574648. http://dx.doi.org/10.1155/2013/574648
9. Renzi M and Guerranti C. Ecotoxicity of nanoparticles in aquatic environment: A review based on multivariate statistic of meta-data. J environ anal chem. 2015. 2:149. doi: 10.4172/2380-2391.1000149.
10. Santschi PH. Marine colloids. Water encyclopedia. 2015. 4: 27-32.

11. Senchenya NG, Guseva TI, and Gololobov YG. Cyanoacrylate-based adhesives. Polymer science series C. 2007. 49(3): 235-239.
12. Dossi M, Storti G, and Moscatelli D. Synthesis of poly(alkyl cyanoacrylates) as biodegradable polymers for drug delivery applications. Macromolecular symposia. 2010. 289: 124-128.
13. Vauthier C, Dubernet C, Fattal E, Pinto-Alphandary H, and Couvreur P. Poly(alkylcyanoacrylates) as biodegradable materials for biomedical applications. Advanced Drug Delivery Reviews. 2003. 55: 519–548.
14. Eaglstein WH and Sullivan T. Cyanoacrylates for Skin Closure. Dermatologic Clinics. 2005. 23: 193 – 198.
15. Bozkurt MK and Saydam L. The use of cyanoacrylates for wound closure in head and neck surgery. European Archives of Oto-Rhino-Laryngology. 2008. 265: 331–335.
16. Shivamurthy DM, Singh S, and Reddy S. Comparison of octyl-2-cyanoacrylate and conventional sutures in facial skin closure. National Journal of Maxillofacial Surgery. 2010. 1(1): 15–19.
17. Romero, I. L., Malta, J. B., Silva, C. B., Mimica, L. M., Soong, K. H., & Hida, R. Y. (2009). Antibacterial properties of cyanoacrylate tissue adhesive: Does the polymerization reaction play a role? *Indian Journal of Ophthamology*, *57*(5), 341-344.
18. Vote BJT and Elder MJ. Cyanoacrylate glue for corneal perforations: a description of a surgical technique and a review of the literature. Clinical and Experimental Opthalmology. 2000. 28: 437-442.
19. Kumari A, Yadav SK, Yadav SC. Biodegradable polymeric nanoparticles based drug delivery systems. Colloids and Surfaces B: Biointerfaces. 2010. 75:1–18.

20. Vauthier C, Dubernet C, Chauvierre C, Brigger I, and Couvreur P. Drug release to resistant tumors: the potential of poly(alkyl cyanoacrylate) nanoparticles. Journal of Control Release. 2003. 93(2): 151-160.
21. Lherm C, Muller R, Puisieux F, and Couvreur P. Alkylcyanoacryalte drug carriers: II. Cytotoxicity of cyanoacrylate nanoparticles with different alkyl chain length. International Journal of Pharmaceutics. 1992. 84: 13–22.
22. Gaspar R, Preat V, Opperdoes FR, and Roland M. Macrophage activation by polymeric nanoparticles of poly-alkylcyanoacrylates: activity against intracellular *Leishmania donovani* associated with hydrogen peroxide production. Pharmaceutical Research. 1992. 9: 782–787.
23. Sulheim E, Baghirov H, Haartman EV, Bøe A, Aslund AKO, Mørch Y, and Lange Davis C. Cellular uptake and intracellular degradation of poly(alkyl cyanoacrylate) nanoparticles. Journal of Nanobiotechnology. 2016. 14:1 https://doi.org/10.1186/s12951-015-0156-7
24. Muller RH, Lherm C, Herbort J, anf Couvreur P. In vitro model for the degradation of alkylcyanoacrylate nanoparticles. Biomaterials. 1990. 11: 590–595.
25. Lao LL, Peppas NA, Boey FYC, and Venkatraman SS. Modeling of drug release from bulk-degrading polymers. International Journal of Pharmaceutical. 2011. 418: 28–41.
26. Gipps E, Groscurt P, Kreuter J, and Speiser PP. The effects of poly(alkylcyanoacrylate) nanoparticles on human normal and malignant mesenchymal cells in vitro. International Journal of Pharmaceutical. 1987. 40: 23-31.

27. Kalhapure RS, Suleman N, Mocktar C, Seedat N, and Govender T. Nanoengineered drug delivery systems for enhancing antibiotic therapy. Journal of Pharmaceutical Science. 2015. 104: 872–905.
28. Álvarez-Paino M, Muñoz-Bonilla A, and Fernández-García M. Antimicrobial Polymers in the Nano-World. Nanomaterials. 2017. 7(48). doi:10.3390/nano7020048
29. Fattal E, Youssef M, Couvreur P, and Andremont A. Treatment of experimental salmonellosis in mice with ampicillin-bound nanoparticles. Antimicrobial Agents and Chemotherapy. 1989. 33(9): 1540-1543.
30. Fresta M, Puglisi G, Giammoma G, Cavalarro G, Micali N, and Furneri PM. Pefloxacine mesilate- and ofloxacin-loaded polyethycyanoacrylate nanoparticles: characterization of the colloidal drug carrier formulation. Journal of Pharmaceutical Science. 1995. 84(7): 895-902.
31. Kisich KO, Gelperina S, Higgins MP, Wilson S, Shipulo E, Oganesyan E, and Heifets L. Encapsulation of moxifloxacin within poly(butyl cyanoacrylate) nanoparticles enhances efficacy against intracellular *Mycobacterium tuberculosis*. International Journal of Pharmaceutical. 2007. 345:154–162.
32. Shirotake S. A new cyanoacrylate colloidal polymer with novel antibacterial mechanism and its application to infection control. Journal of Nanomedicine and Biotherapeutic Discovery. 2014. 4(1): 1-7.
33. Miao AJ, Schwehr KA, Xu C, Zhang SJ, Luo Z, Quigg A, and Sanstchi PH. The algal toxicity of silver engineered nanoparticles and detoxification by exopolymeric substances. Environmental Pollution. 2009. 157(11): 3034-3041

34. Libralato G, Galdiero E, Falanga A, Carotenuto R, de Alteriis E, and Guida M. Toxicity effects of functionalized Quantum Dots, gold, and polystyrene nanoparticles on target biological models: A review. Molecules. 2017. 22: 1439
35. Miazek K, Iwanek W, Remacle C, Richel A, and Goffin D. Effect of metals, metalloids, and metallic nanoparticles on microalgae growth and industrial product biosynthesis: a review. International Journal of Molecular Sciences. 2015. 16(10): 23929-23969.
36. Quigg A, Chin W, Chen C, Zhang S, Jiang Y, Miao A, Schwehrll KA, and Santschi PH. Direct and indirect toxic effect of engineered nanoparticles on Algae: Role of natural organic matter. ACS Sustainable Chemistry and Engineering. 2013. 1: 686-702
37. Navarro E, Piccapietra F, Wagner B, Marconi F, Kaegi R, Odzak N, Sigg L, and Behra R. 2008. A toxicity of silver nanoparticles to *Chlamydomonas reinhardtii*. Environmental Science and Technology. 2008. 42: 8959-8964
38. Pillai S, Behra R, Nestler H, Suter MJ, Sigg L, and Schirmer K. Linking toxicity and adaptive responses across the transcriptome, proteome, and phenotype of Chlamydomonas reinhardtii exposed to silver. PNAS. 2014. 111(9): 3490-3495
39. Miao A, Luo Z, Chen C, Chin W, Sanstchi PH, and Quiqq A. Intracellular uptake: A possible mechanism for silver engineered nanoparticle toxicity to a freshwater alga *Ochromonas Danica*. Plos one. 2010. 5(12). https://doi.org/10.1371/journal.pone.0015196
40. Renault S, Baudrimont M, Mesmer-Dudons N, Gonzalez P, Mornet S, and Brisson A. Impacts of gold nanoparticle exposure on two freshwater species: a phytoplanktonic alga (*Scenedesmus subspicatus*) and a benthic bivalve (*Corbicula fluminea*). Gold Bulletin. 2008. 41:116–126

41. Van Hoecke K, De Schamphelaere KAC, Ali Z, Zhang F, Elsaesser A, Rivera-Gil P, Parak WJ, Smagghe G, Howard CV, and Janssen CR . Ecotoxicity and uptake of polymer coated gold nanoparticles. Nanotoxicology. 2013. 7: 37–47
42. Behra R, Wagner B, Sgier L, and Kristler D. Colloidal stability and toxicity of gold nanoparticles and gold chloride on *Chlamydomonas reinhardtii*. Aquatic Geochemistry. 2015. 21: 331-342.
43. Hund-rinke K and Simon M. Ecotoxic effect on photocatalytic active nanoparticles TiO2 on algae and daphnids. Environmental Science and Pollution Research. 2006. 17(5): 372-386
44. Aruoja V, Dubourguier HC, Kasemets K, and Kahru A. Toxicity of nanoparticles of CuO, ZnO, and TiO2 to microalgae *Pseudokirchneriella subcapitata*. Science of The Total Environment. 2009. 407(4): 1461-1468
45. Franklin NM, Rogers NJ, Apte SC, Batley GE, Gadd GE, and Casey PS. Comparative toxicity of nanoparticulate ZnO, Bulk ZnO, and ZnCl2 to a freshwater microalga (*Pseudokirchnereilla subcapitata*): the importance of particle solubility. Environmental Science and Technology. 2007. 41(24): 8484-8490.
46. Chen P, Powell BA, Mortimer M, and Ke PC. Adaptive interactions between zinc oxide nanoparticles and Chlorella sp. Environmental Science and Technology. 2012. 46(21): 12178-12185.
47. Basiuk EV, Ochoa-Olmos OE, De la Mora-Estrada LF. Ecotoxicological effects of carbon nanomaterials on algae, fungi, and plants. Journal of Nanoscience and Nanotechnology. 2011. 11(4): 3016-3038.

48. Schwab F, Bucheli TD, Lukhele LP, Magrez A, Nowack B, Sigg L, and Knauer K. Are carbon nanotube effects on green algae caused by shading and agglomeration? Environmental Science and Technology. 2011. 45: 6136-6144.

49. Sohn EK, Chung YS, Johari SA, Kim TG, Kim JK, Lee JH, Lee YH, Kang SW, and Yu IJ. Acute toxicity comparison of single-walled carbon nanotubes in various freshwater organisms. BioMed Research International. 2015. Article ID 323090. http://dx.doi.org/10.1155/2015/323090.

50. Luo J. Toxicity and bioaccumulation of nanomaterial in aquatic species. Journal of U.S Stockholm Junior Water Prize. 2007. 2: 1-16.

51. Matorin DN, Karateyeva AV, Osipov VA, Lukashev EP, Seifullina NKh, and Rubin AB. Influence of carbon nanotubes on chlorophyll fluorescence parameters of green algae *Chlamydomonas reinhardtii*. Nanotechnologies in Russia. 2010. 5:320-327.

52. Sjollema SB, Redondo-Hasselerharm P, Leslie HA, Kraak MHS, and DickVethaak A. Do plastic particles affect microalgal photosynthesis and growth?. Aquatic toxicology. 2016. 170: 259-261.

53. Nolte TM, Hartmaan NB, Klejin JM, Garnæs J, van de Meent D, Hendriks AJ, and Baun A. The toxicity of plastic nanoparticles to green algae as influenced bysurface modification, medium hardness and cellular adsorption. 2017. Aquatic toxicology. 2017. 183: 11-20.

54 Bhattacharya P, Lin S, Turner JP, and Ke PC. Physical Adsorption of Charged Plastic Nanoparticles Affects Algal Photosynthesis. Journal of Physics and Chemistry series C. 2010. 114: 16556-16561.

55. Li X. Interactions of silver and polystyrene nanoparticles with algae. Doctoral Dissertation. 2015. Retrieved from: https://infoscience.epfl.ch/record/213652.

CHAPTER 2. Acutely induced cell mortality in the unicellular green alga *Chlamydomonas reinhardtii* (Chlorophyceae) following exposure to acrylic resin nanoparticles

2.1 Introduction

Nanoparticles (NPs) have substantially different properties from bulk materials of the same composition, largely due to their large surface area per unit mass. The particle size and surface chemistry of NPs are crucial determinants of their reactivity and toxicity, as an increased surface area allows them to strongly interact with biological tissues and natural organic matter in the environment, and their surface properties affect the way in which they aggregate and are deposited in aquatic systems [1-3].

The unique properties of NPs make them attractive for use in industrial and medical technology industries. However, these same properties can also be harmful to living organisms and the environment, with previous experiments having shown that the presence of NPs in aquatic test systems leads to decreased fertility, physiological changes, abnormal behaviors, and an increased mortality rate in aquatic organisms [1,4-5]. Therefore, there is an urgent need to better understand the molecular mechanisms that are involved in the interactions between NPs and biological systems, and any other risks they pose to the environment.

Unicellular algae are basic organisms that are fundamental components of aquatic ecosystems, and so it is essential that we gain an understanding of how NPs affect their physiology. It has previously been suggested that metal oxide NPs have a toxic effect on unicellular algae due to their adsorption onto the algal cell wall, the generation of ROS, the release of metal ions, and the simultaneous effects of various other factors [6-8]. It

has also been reported that carbon nanotubes (CNTs) and polystyrene nanoparticles (PS-NPs) have limited toxic effects in unicellular algae such as *Chlorella vulgaris* and *Pseudokirchneriella subcapitata*. These effects include impaired growth and reduced photosynthetic activity, and are thought to be caused by oxidative stress as a result of shading and agglomeration in the case of CNTs [9-11], and adsorption on the algal cell wall and the formation of algae–NP agglomerates in the case of PS-NPs. Indeed, it is often speculated that shading is the primary cause of reduced viability in phototrophic organisms following exposure to NPs [12-13].

Recently, there has been an increased interest in NPs made of polyalkylcyanoacrylates for use as biodegradable drug carriers due to their ease of fabrication and functionalization, biocompatibility, sustained drug release, and controllable degradation rate [14-15]. Shirotake [16] also reported that NPs made of poly *n*-butyl cyanoacrylate could induce bacteriolysis in various Gram-positive bacteria, such as *Staphylococcus aureus* and *Entrococci* sp., without binding to an antibiotic, but had no effect on Gram-negative bacteria. However, it remains unknown why acrNPs can only induce cell lysis in Gram-positive bacteria.

In the present study, we examined the effects of three different sized acrNPs made of poly(isobutyl-cyanoacrylate) on the unicellular green alga *Chlamydomonas reinhardtii*. We then investigated the possible mechanisms of action by examining the effects of acrNPs on three different strains of *C. reinhardtii* with various levels of cell wall development.

2.2 Materials and methods

2.2.1 Nanoparticles

Three different sized acrNPs (25 nm, 180 nm, and 350 nm in diameter) made of poly(isobutyl-cyanoacrylate) were kindly supplied by CHIKAMI MILTEC INC. (Kochi, Japan). acrNPs with a mean diameter of approximately 25 nm [hereafter, acrNP(25 nm)] were supplied as a 1% (w/v) suspension in water containing 1.25% (w/v) of the non-ionic surfactant RHEODOL TW-L (Kao Corporation, Tokyo, Japan) and 1.0% (w/v) of the anionic surfactant NEOPELEX G-15 (Kao Corporation) as dispersants; acrNP(180 nm) was supplied as a 1% (w/v) suspension in water containing 1.0% (w/v) dextran 60,000 (041-30525; Wako Pure Chemical Industries, Osaka, Japan); and acrNP(350 nm) was supplied as a 1% (w/v) suspension in water containing 3.0% (w/v) PEG 20,000 (168-11285; Wako Pure Chemical Industries). All of the dispersed diameter values were based on measurements taken immediately after production using the dynamic light scattering (DLS) method. Data sheets were kindly provided by CHIKAMI MILTEC INC. (Table 2.1).

Table 2.1. Particle size and zeta potential of acrNPs in dispersing reagents

Dispersants	Size (mean ± S.D.) (nm)	Zeta potential (mV)
RHEODOL TW-L 120 NEOPELEX G-15	24.9 ± 7.6	-10.0
Dextran 60,000	183.3 ± 77.6	-3.80
PEG 20,000	351.3 ± 102.3	-15.0

Plain polystyrene NPs with an average diameter of 50 nm [hereafter, PS-NP(50 nm)] were supplied by Polysciences Inc. (Philadelphia, USA), while the metal oxide NPs that were used in this study were ZnO (544906; Sigma), which contains particles of <100 nm, and TiO_2 (anatase form) (205-01715; Wako Pure Chemical Industries).

2.2.2 Ultra-filtrate of acrNP(180 nm)

To prepare a filtrate from which almost all of the acnNP(180 nm) had been removed, we used Ultra-15 Centrifugal Filter Units with a 10,000 nominal molecular weight limit (Amicon).

2.2.3 Algal strain and culture condition

The algal strains that were used in this study are summarized in Table 2.2 and were classified according to the National Institute of Environmental Studies (NIES) system (http://mcc.nies.go.jp/index_en.html). Three *C. reinhardtii* strains were provided by the *Chlamydomonas* Resource Center at the University of Minnesota (MN, USA): (1) the wild type, CC-124; (2) a mutant with very thin cell walls, CC-503 (*cw9*); and (3) a mutant with no cell walls, CC-400 (*cw15*) [17-18]. These strains were cultured under constant fluorescent light (84 μmol photons $\cdot$ $m^{-2} \cdot s^{-1}$) with gentle shaking in Tris-acetate-phosphate (TAP) medium (pH 7.0) [19]. The remaining samples were obtained from the Microbial Culture Collection at NIES (Tsukuba, Japan) and cultured in the media and conditions recommended by NIES. Unless otherwise stated, cells at the mid-log phase ($OD_{750} \approx 0.8$) were used in all experiments.

Table 2.2 List of green algal species and their sensitivity to acrNP

Name of species	Strain	Classification
Astrephomene gubernaculifera	NIES-418	Chlorophyceae, Volvocales, Reinhardtinia, Goniaceae
Carteria crucifera	NIES-421	Chlorophyceae, Volvocales, Crucicarteria
Carteria radiosa	NIES-432	Chlorophyceae, Volvocales, Radicarteria
Chlamydomonas applanata	NIES-2202	Chlorophyceae, Volvocales, Polytominia
Chlamydomonas assymetrica	NIES-2208	Chlorophyceae, Volvocales, Reinhardtinia

Chlamydomonas debaryana	NIES-2212	Chlorophyceae, Volvocales, Reinhardtinia
Chlamydomonas globosa	NIES-2462	Chlorophyceae, Volvocales, Reinhardtinia
Chlamydomonas moewusii	NIES-2578	Chlorophyceae, Volvocales, Moewusinia
Chlamydomonas monadina	NIES-438	Chlorophyceae, Monadinia
Chlamydomonas noctigama	NIES-1048	Chlorophyceae, Volvocales, Moewusinia
Chlamydomonas parkeae	NIES-1022	Chlorophyceae, Volvocales, Moewusinia
Chlamydomonas perpusilla	NIES-1848	Chlorophyceae, Volvocales, Chlorogonia
Chlamydomonas reinhardtii	CC-124,CC-503, CC-400	Chlorophyceae, Volvocales, Reinhardtinia
Chlorella ellipsoide	NIES-2150	Trebouxiophyceae
Chlorella saccharophila	NIES-2352	Trebouxiophyceae
Chlorella sorokiniana	NIES-2169	Trebouxiophyceae
Chlorella vulgaris	NIES-2170	Trebouxiophyceae
Chloromonas actinochloris	NIES-2201	Chlorophyceae, Volvocales, Chloromonadia
Dysmorphococcus globosus	UTEX LB-65	Chlorophyceae, Volvocales
Eudorina elegans	NIES-456	Chlorophyceae, Volvocales, Reinhardtinia, Volvocaceae
Euglena gracilis	NIES-49	Euglenophyceae
Gonium multicocum	NIES-737	Chlorophyceae, Volvocales, Reinhardtinia, Goniaceae
Haematococcus lacustris	NIES-144	Chlorophyceae, Volvocales, Chlorogonia
Labochlamys culleus	NIES-2209	Chlorophyceae, Oogamochlamydinia
Pandorina morum	NIES-362	Chlorophyceae, Volvocales, Reinhardtinia, Volvocaceae
Phacotus lenticularis	NIES-858	Chlorophyceae, Volvocales, Phacotinia

Pseudokirchneriella subcapitata	NIES-35	Chlorophyceae, Sphaeropleales, Selenastraceae
Scenedesmus obliquus	NIES-2280	Chlorophyceae, Sphaeropleales, Scenedesmaceae
Tetrabaena socialis	NIES-571	Chlorophyceae, Volvocales, Reinhardtinia, Tetrabaenaceae
Volvox carteri	NIES-732	Chlorophyceae, Volvocales, Reinhardtinia, Volvocaceae
Volvulina steiniii	NIES-545	Chlorophyceae, Volvocales, Reinhardtinia, Volvocaceae

2.2.4 Zeta potential and size distribution

The acrNPs were diluted with TAP (pH 7.0) to give a final concentration of 100 mg · L^{-1} or 250 mg · L^{-1} and left for 4 hours. The effective surface charge (zeta potential), particle size distribution, and polydispersity index (PDI) of the particles were then measured using the DLS method with a Zetasizer (Nano ZS90; Malvern Instruments). These parameters were also analyzed for PS-NPs, ZnO-NPs, and TiO_2-NPs at final concentrations of 100 mg · L^{-1} in TAP, as were the zeta potentials of exponentially growing cells of the *C. reinhardtii* strains CC-124, CC-503, and CC-400 in TAP.

2.2.5 Dispersion stability

The dispersion stability of the acrNPs was determined by measuring their absorbance at 221 nm, which represented maximum absorbance, using an ultraviolet-visible spectrophotometer. Each of the three acrNPs (25 nm, 180 nm, and 350 nm) was diluted in TAP to give a final concentration of 250 mg · L^{-1} and placed in a 50-cm tube. The absorbance of the top 0.5–1-cm layer of the solution was then measured each hour over 6 hours following the Organization for Economic Co-operation and Development

manual to analyze the dispersion stability. The percentage change in dispersion over time was then determined using the following equation:

$$\%\ initial\ = \frac{At}{A_0} \times 100\ \%$$

where A_0 is the initial absorbance at 0 hours and A_t is the absorbance at a particular time point. This experiment was carried out in triplicate for each acrNP.

2.2.6 Scanning electron microscopy (SEM) observation of acrNP(180 nm)

acrNP(180 nm) was added to absolute ethanol, precipitated by centrifugation (15,000 × *g*, 15 minutes), and then dried using a vacuum dryer. The resulting dehydrated acrNP(180 nm) was sputter coated with platinum and examined under a scanning electron microscope (JSM-6701F; JEOL Ltd, Tokyo, Japan) using an accelerating voltage of 3.0 kV.

To observe cross-sections of acrNP(180 nm), 0.25 ml of a suspension in water [1% (w/v)] was mixed with 1.25 ml of 5% polyvinyl alcohol (dissolved in water) and dried at 40°C. The embedded acrNP(180 nm) was then cut using a surgical knife.

2.2.7 Exposure of algal cells to acrNPs

To assess the potential physiological effects of acrNPs on algal cells, three experiments were carried out in which various strains of *C. reinhardtii* were exposed to a wide range of concentrations of the three different sized acrNPs.

Experiment 1: To analyze the effect of acrNP concentration and the presence of a cell wall on the cell mortality ratio, each strain of *C. reinhardtii* was exposed to the three acrNPs at final concentrations of 250 mg · L^{-1}, 500 mg · L^{-1}, and 1,000 mg · L^{-1} for 4 hours.

Experiment 2: To analyze the effect of the molar concentration and total surface area of acrNPs on cell mortality, wild-type *C. reinhardtii* cells were exposed to various concentrations of acrNPs. Since the molecular weight of the acrNPs is unknown, we adjusted the concentrations using the weight per unit volume to allow us to use the same relative molar concentration for each of the different sized acrNPs. The relative weight ratio of acrNP(25 nm):acrNP(180 nm):acrNP(350 nm) was found to be 25^3:180^3:350^3, based on these acrNPs being made of the same material and uniformly solid (Table S1). Thus, 25^3 mg · L^{-1} of acrNP(25 nm), 180^3 mg · L^{-1} of acrNP(180 nm), and 350^3 mg · L^{-1} of acrNP(350 nm) have the same molar ratio per liter [e.g., acrNP(25 nm):acrNP(180 nm):acrNP(350 nm) = 1 mg · L^{-1}:373 mg · L^{-1}:2,744 mg · L^{-1}].

If the three acrNPs have the same weight despite being different sizes, the total surface area ratio of acrNP(25 nm):acrNP(180 nm):acrNP(350 nm) will be $25^2\times(1/25^3)$:$180^2\times(1/180^3)$:$350^2\times(1/350^3)$. Thus, for example, 25 mg · L^{-}1 of acrNP(25 nm), 180 mg · L^{-1} of acrNP(180 nm), and 350 mg · L^{-1} of acrNP(350 nm) will have the same total surface area. Since the apparent diameters of the acrNPs gradually increased in the original stock solution over time, we used the mean diameters that were measured immediately after production (Table S1) in these calculations.

Based on this information, we used three sets of conditions in which the molar concentration of acrNP was the same independent of the particle size. In these three sets of conditions, the acrNPs had the following weight per unit volume concentrations: condition 1, 0.5 mg · L^{-1} of acrNP(25 nm), 187 mg · L^{-1} of acrNP(180 nm), and 1,372 mg · L^{-1} of acrNP(350 nm); condition 2, 1 mg · L^{-1} of acrNP (25 nm), 374 mg · L^{-1} of acrNP (180 nm), and 2,744 mg · L^{-1} of acrNP (350 nm); and condition 3, 1.5 mg · L^{-1} of acrNP (25 nm), 561 mg · L^{-1} of acrNP (180 nm), and 4,116 mg · L^{-1} of acrNP (350 nm).

Similarly, we used three sets of conditions in which the total surface area of the acrNPs was the same independent of the particle size. In these three sets of conditions, the acrNPs had the following weight per volume concentrations: condition 1, 35.63 mg · L^{-1} of acrNP(25 nm), 255.5 mg · L^{-1} of acrNP(180 nm), and 500 mg · L^{-1} of acrNP(350 nm); condition 2, 71.25 mg · L^{-1} of acrNP(25 nm), 511 mg · L^{-1} of acrNP(180 nm), and 1,000 mg · L^{-1} of acrNP(350 nm); and condition 3, 142.5 mg · L^{-1} of acrNP(25 nm), 1,022 mg · L^{-1} of acrNP(180 nm), and 2,000 mg · L^{-1} of acrNP(350 nm).

Experiment 3: To analyze the generation of ROS, wild-type *C. reinhardtii* cells were exposed to acrNP(25 nm), PS-NPs, and metal oxide NPs at final concentrations of 100 mg · L^{-1} for 3 hours.

In each experiment, the cells were exposed to the NPs by placing them in 1.5-ml or 5-ml sample tubes, which were placed on their sides in dim light and very gently rotated (10 rpm). We also incubated the cells in TAP medium containing dispersant solutions that were used in the acrNP preparation to determine whether these reagents had toxic effects on the cells.

2.2.8 Trypan blue staining assay

To differentiate live cells from dead ones, we used a trypan blue staining assay. Trypan blue solution [0.4% (w/v); Wako Chem., Japan] was added directly to samples at a final concentration of 0.2% (w/v). Following incubation for five minutes, a drop of algal culture was placed on a glass microscope slide, then the color of the cytoplasm was observed without washing. To calculate the cell mortality ratio, we counted the total number of blue-stained cells observed out of 100 cells.

2.2.9 Transmission electronic microscopy (TEM) observation of *Chlamydomonas* exposed to acrNP(25 nm)

Chlamydomonas CC-124 cells were co-incubated with acrNP(25 nm) at a concentration of 65 mg/L in TAP for 15 min [hereafter, acrNP(25 nm|65 mg/L|15 min)]. Then, treated cells were collected by centrifugation (2,000 × g, 5 min). Collected cells were fixed for 4 h at 4°C in 1/15 M phosphate buffer (pH 7.4), containing 4 % glutaraldehyde. They were then washed for one hour with 1/15 M phosphate buffer (pH 7.4) at 4°C. Cells were pre-fixed for two hours at 4°C in phosphate buffer containing 2% osmium tetroxide, then washed for one hour with distilled water at 4°C. They were then stained with 2% uranyl acetate at 4°C. Cells were dehydrated in ethanol by gradually increasing the ethanol concentration and temperature and then embedded in Quetol 651（Polysciences, USA）. Ultra-thin sections were stained with 2% uranyl acetate for 5 min at room temperature and then stained a second time with lead citrate for 10 min at room temperature. Electron microscopic observation was accomplished by Hitachi H-7650 using an accelerating voltage of 80 kV.

2.2.10 Reactive oxygen species (ROS) generation analyses

In this study, we always observed fading of the green coloration of *C. reinhardtii* cells following exposure to acrNPs, suggesting that the chloroplasts may have been damaged. Therefore, since damaged active photosynthetic systems can be a major source of ROS generation, we compared the ROS levels in wild-type *C. reinhardtii* (CC-124) cultured under light and dark conditions.

We detected differences in the ROS levels that were generated by cells of the wild-type strain of *C. reinhardtii* (CC-124) cultured under light or dark conditions as follows. First, 5 ml of culture containing cells in the exponential growth phase was separated

into two aliquots. One of these aliquots was diluted 100 times with Tris-minimal medium (pH 7.0 with HCl adjustment) (Gorman & Levine 1965) and cultured under constant light, while the other was diluted with TAP and kept in the dark. Both cultures were then maintained until they reached the mid-exponential growth phase, at which time acrNP(25 nm|100 mg · L^{-1}) was added and culture was continued for 3 hours under the same conditions (i.e., constant light or dark).

The presence of ROS was detected using 2',7'-dichlorodihydrofluorescein diacetate (H2DCFDA) (D668, Sigma). This cell-permeable, non-fluorescent compound is converted to the highly fluorescent 2',7'-dichlorofluorescein (DCF) by ROS in the cytoplasm, the intensity of which is proportional to the amount of ROS (Szivák et al. 2009, Wojtala et al. 2014). Thus, we added H2DCFDA solution (10 µM final concentration) to each sample, left it for 15 minutes, and then washed it in TAP three times to reduce the background intensity. We then viewed part of the sample under an Olympus IX71 fluorescence microscope to directly observe ROS and the remaining part of the sample under a fluorescence spectrophotometer (FL-2500; Hitachi, Japan) at a wavelength of Ex/Em = 495/515 nm to measure the fluorescence of DCF. This procedure was repeated every hour.

This method was also used to detect ROS levels in *C. reinhardtii* cells that had been exposed to PS-NPs, and metal oxide NPs.

2.2.11 Data analysis and statistic

The cell mortality ratios and ROS generation levels for each group were compared using one-way analysis of variance or student's t-test, and the differences between the means were then inspected with Tukey's test for *post hoc* multiple comparisons. The differences between means were considered statistically significant when the p-value

was < 0.05. The similarities of the cell mortality profiles of the three strains following exposure to the same molar concentrations or the same total surface area inputs for the three different sized acrNPs were examined using Pearson correlation analysis, whereby the correlation was considered strong when the correlation coefficient (r) was close to 1. All data were analyzed using GraphPad Prism version 7.03 (GraphPad Software, San Diego, California, USA) and are presented as means ± standard errors (SE).

2.3 Results

2.3.1 Physicochemical characteristics of acrNPs

Analysis of the zeta potential of the three different sized acrNPs in the TAP medium showed that acrNP(25 nm) was slightly negatively charged (−15.63 ± 0.917 mV), while acrNP(180 nm) and acrNP(350 nm) were much closer to neutral (−1.353 ± 0.259 mV and −3.473 ± 0.249 mV at 250 mg · L^{-1}, respectively), with no significant difference between concentrations (100 mg · L^{-1} vs. 250 mg · L^{-1}) (Table 2.3).

DLS showed that the mean diameters of the acrNPs after being suspended in TAP medium for 4 hours were 63.45 ± 0.090 nm for acrNP(25 nm), 202.55 ± 0.070 nm for acrNP(180 nm), and 1,919 ± 21.21 nm for acrNP(350 nm) at 250 mg · L^{-1}, which was again similar to the results at 100 mg · L^{-1} (Table 3). PDI (Table 3) and size distribution (Fig. 2.1A) analyses using the Zetasizer showed that most of the acrNP(25 nm) and acrNP(180 nm) particles were monodisperse, with a uniform and rather narrow size distribution, even after 4 hours in TAP media, whereas acrNP(350 nm) had a broader size distribution (Fig. 2.1A) and higher PDI value.

Table 2.3 Zeta potential, Mean diameter size and polydispersity index (PDI) of of acrNPs, PSNP, ZnO-NP, and TiO_2-NP on Tris-acetate-phosphate (TAP, pH 7.0)

Particle	Concentration (mg • L^{-1})	Zeta potential ± SD (mV)	Size ± SD (nm)	PDI ± SD
acrNP(25 nm)	250	-15.63 ± 0.917	63.45 ± 0.090	0.155 ± 0.009
acrNP(180 nm)		-1.353 ± 0.259	202.55 ± 0.070	0.302 ± 0.011
acrNP(350 nm)		-3.473 ± 0.249	1919 ± 21.21	0.73 ± 0.151
acrNP(25 nm)	100	-14.5 ± 2.970	62.78 ± 0.26	0.153 ± 0.003
acrNP(180 nm)		-1.337 ± 0.130	205.1 ± 6.428	0.274 ± 0.026
acrNP(350 nm)		-3.84 ± 0.088	1181 ± 176	0.609 ± 0.159
PSNP(50 nm)		-28.97 ± 1.558	53.62 ± 0.311	0.062 ± 0.0028
ZnO-NP		-17.93 ± 0.249	2279 ± 118.01	0.481 ± 0.044
TiO_2-NP		-15.7 ± 0.163	1823 ± 40.80	0.396 ± 0.0971

We determined the dispersion stability of the acrNPs by measuring the time-dependent changes in absorbance in the upper layer (Fig. 2.1B). We found that there was no marked decrease in absorbance for acrNP(25 nm) or acrNP(180 nm) even after 6 hours in TAP (ca. 98% of the initial absorbance), suggesting that these acrNPS formed a stable suspension. By contrast, the absorbance constantly decreased over time for acrNP(350 nm), being ca. 63% of the initial value at 6 hours after dilution in TAP, suggesting the formation of aggregates. SEM observation of acrNP(180 nm) and its cross-section clearly showed that it-had a spherical outer shape and a solid structure (Fig. 2.1C).

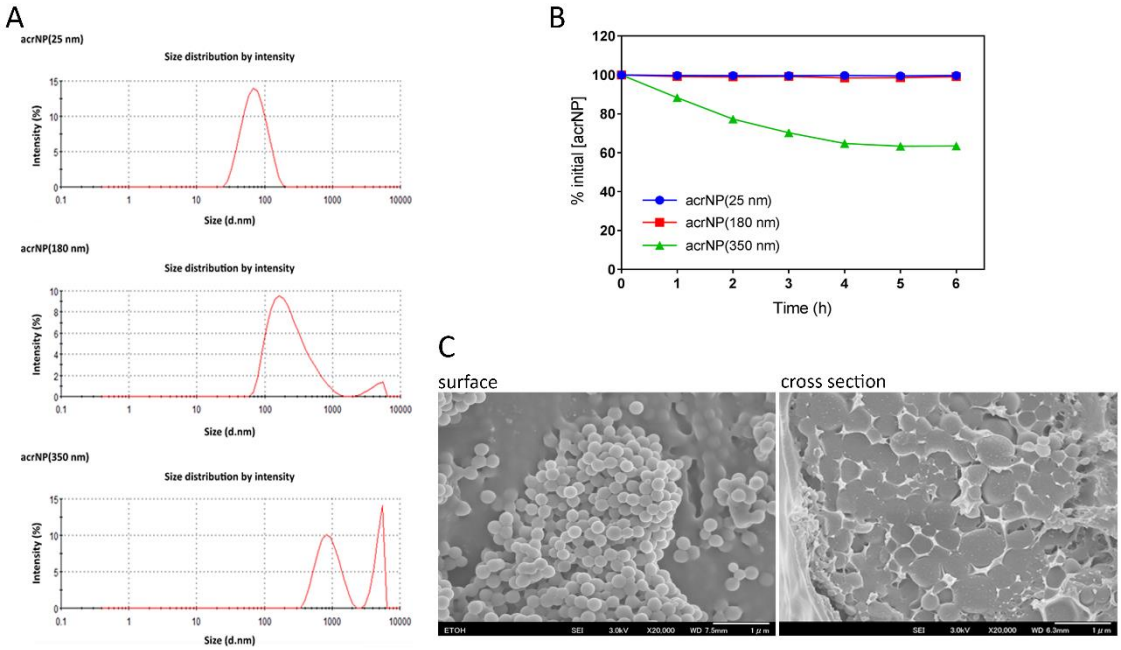

Fig. 2.1 Physicochemical characteristics of acrylic resin nanoparticles (acrNPs). (A) Particle size distribution and (B) dispersion stability of three different sized acrNPs (25 nm, 180 nm, and 350 nm in diameter) in Tris-acetate-phosphate (TAP, PH 7.0) medium. (C) Scanning electron microscope observation of acrNP(180 nm) and its cross-section.

2.3.2 Zeta potential of *C. reinhardtii* cells

The zeta potentials of the three strains of *C. reinhardtii* in TAP during the exponential growth phase were very similar (CC-124, −8.45 ± 1.54 mV; CC-503, −7.01 ± 0.361 mV; and CC-400, −7.52 ± 0.041 mV), despite their different cell wall conditions.

2.3.3 Effects of acrNP to on the swimming behavior of *Chlamydomonas reinhardtii*

Following exposure to acrNP(180 nm) at a concentration of 100 mg · L^{-1} [hereafter, acrNP(180 nm|100 mg · L^{-1})], the first response that was observed in the wild-type *C. reinhardtii* strain CC-124 was a change in swimming pattern, which occurred immediately. The ordinarily smooth swimming orbit exhibited abrupt and frequent

directional changes, followed by a twirling motion on the spot (Video 2.1). We also noticed that the original ellipsoidal shaped wild-type cells quickly became spherical and swollen (Video 2.2), and that some of these burst open, resulting in extrusion of the cytosol. This implied that these inflated, spherical cells were osmotically fragile protoplasts or had only very thin cell walls (spheroplasts).

Direct observation of the trails of acrNP(180 nm) using dark field microscopy showed that acrNP(180 nm) particles occasionally collided with the cells and bounced (Video 2.1), with no noticeable particles becoming entrapped on the cell surface.

These rapid and abnormal phenomena were observed for all three acrNPs (25 nm, 180 nm, and 350 nm in diameter). By contrast, cells that were maintained in the control medium, which contained only the dispersants that were used to prepare the acrNPs, maintained normal swimming patterns. We also confirmed that the ultra-filtrate of acrNP(180 nm) did not induce abnormal swimming patterns or cause cell lysis, indicating that these responses were caused by larger acrNP particles that were not contained in the ultrafiltration filtrate.

2.3.4 Effect of acrNPs on cell mortality

The trypan blue staining assay repeatedly showed that acrNPs potentially caused acute cell mortality in *C. reinhardtii*. There was a significant positive relationship between the mass concentration (w/v) of acrNPs and the cell mortality ratio for all three sizes of acrNPs ($p < 0.05$). For example, the cell mortality ratio was ca. 30% after 1 hour's exposure to acrNP(25 nm|250 mg · L^{-1}) but ca. 97% after 1 hour's exposure to acrNP(25 nm|500 mg · L^{-1}) or acrNP(25 nm|1,000 mg · L^{-1}) (Fig 2.2).

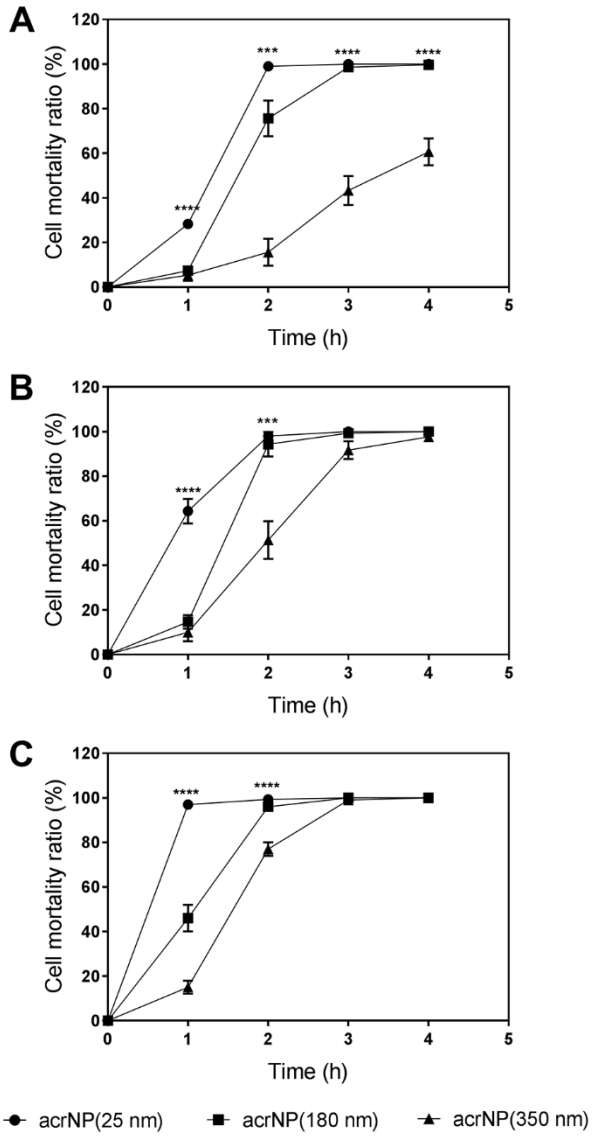

Fig. 2.2 Induced cell mortality ratios in exponentially growing wild-type *Chlamydomonas reinhardtii* cells following exposure to three different sized acrylic resin nanoparticles (acrNPs). Cell mortality ratios are shown following exposure to three different sized acrNPs (25 nm, 180 nm, and 350 nm in diameter) at concentrations of (A) 250 mg · L^{-1}, (B) 500 mg · L^{-1}, and (C) 1,000 mg · L^{-1}. Cell mortality ratios were calculated as the number of trypan blue stained and lysed cells observed out of 100 total cells. Results are shown as mean ratios (± SE) from three independent experiments. Asterisks denote significant differences between the acrNPs at a particular time point (one-way analysis of variance, **** $p < 0.0001$).

There was also a significant negative relationship between the size of the acrNPs and the cell mortality ratio at a given mass concentration, particularly during the first 2

hours' exposure at concentrations of 250 mg · L^{-1}, 500 mg · L^{-1}, and 1,000 mg · L^{-1} (Fig. 2). Thus, at a given mass concentration, acrNP(25 nm) had the greatest effect on inducing cell death, while acrNP(350 nm) had the least effect. For example, after 2 hours' exposure to a concentration of 250 mg · L^{-1} (Fig. 2.2A), the cell mortality ratio reached 99% with acrNP(25 nm), ca. 75% with acrNP(180 nm), and only 20% with acrNP(350 nm).

It is worth noting that overgrown cells in the stationary phase (OD_{750} = 1.7) were much less sensitive to all three acrNPs at a concentration of 250 mg · L^{-1} than cells in the exponential growth phase. For example, after 2 hours' exposure to acrNP(25 nm|250 mg · L^{-1}), the ratio of trypan blue stained cells was only 13% for cells in the stationary phase compared with 99% for exponentially growing cells (Fig. 2.3).

2.3.5 Sensitivity of cell wall mutants to acrNPs

Cell lysis was frequently observed in strain CC-400, which lacked a cell wall, but was observed at a much lower rate in strain CC-503, which had a very thin cell wall. After 1 hour's exposure to acrNP(25 nm|250 mg · L^{-1}), the cell mortality ratio reached ca. 95% in strain CC-400, compared with ca. 41% in strain CC-503 and 28% in the wild-type strain CC-124. It is also worth noting that cell mortality increased much more acutely in CC-400 than in CC-124 or CC-503 (Fig. 2.4).

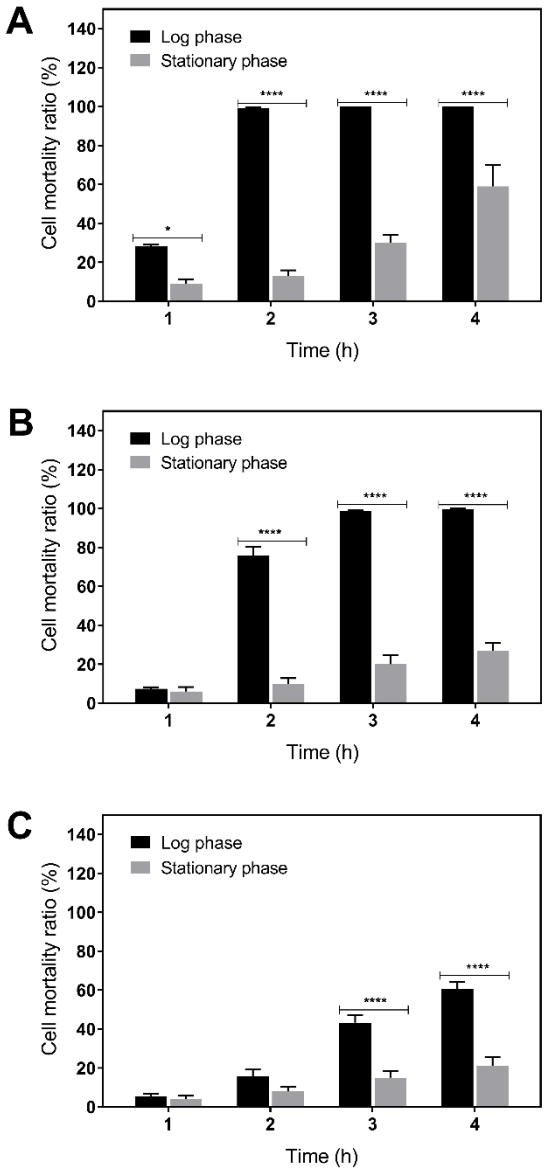

Fig. 2.3 Induced cell mortality ratios in exponentially growing and stationary phase wild-type *Chlamydomonas reinhardtii* cells following exposure to acrylic resin nanoparticles (acrNPs). Cells were exposed to three different sized acrNPs: (A) 25 nm, (B) 180 nm, and (C) 350 nm in diameter at a concentration of 250 mg · L^{-1} each. Cell mortality ratios were calculated as the number of trypan blue stained and lysed cells observed out of 100 total cells. Results are shown as mean ratios (± SE) from three independent experiments. Asterisks denote significant differences between the log phase and stationary phase (t-test, * $p < 0.05$, **** $p < 0.0001$).

A repeated assay clearly demonstrated that the mortality rate per unit time exposed to acrNP was highest in CC-400 and lowest in CC-124, regardless of the acrNP particle

size used, which suggests that the cell wall was functioning primarily as a structural barrier to inhibit cell death. This was especially obvious in the early period of the exposure.

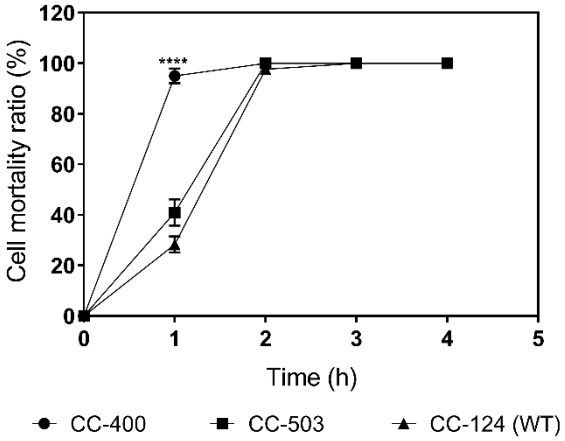

Fig. 2.4 Time course of cell mortality ratios in three strains of *Chlamydomonas reinhardtii* following exposure to acrylic resin nanoparticles (acrNPs). The wild-type strain CC-124, a thin cell wall-bearing mutant CC-503, and a cell wall-lacking mutant CC-400 were exposed to acrNP(25 nm) at a concentration of 250 mg · L^{-1}. The cell mortality ratio was calculated as the number of trypan blue stained cells observed out of 100 total cells. Results are shown as mean ratios (± SE) from three independent experiments. Asterisks denote significant differences between the strains at a given time (one-way analysis of variance, **** $p < 0.0001$).

2.3.6 Effect of molar concentration and surface area of acrNPs on cell mortality

For all three sets of conditions in which a constant molar concentration was used independent of particle size, both acrNP(180 nm) and acrNP(350 nm) had different effects on the cell mortality ratio from acrNP(25 nm) [Fig. 2.5A(a–c)]. For example, under the second set of conditions, acrNP(180 nm|374 mg · L^{-1}) and acrNP(350 nm|2,744 mg · L^{-1}) had similar cell mortality profiles (Pearson's correlation coefficient, $r = 0.99$), whereby the cell mortality ratio increased with increasing exposure time, whereas acrNP(25 nm|1 mg · L^{-1}) had a weak similarity to the cell mortality profiles of

both acrNP(180 nm|374 mg · L^{-1}) and acrNP(350 nm|2,744 mg · L^{-1}) (Pearson's correlation coefficients, r = 0.45 and 0.378, respectively). Moreover, the cell mortality ratio was significantly lower with acrNP(25 nm) than with acrNP(180 nm) or acrNP(350 nm) over the exposure time for all three sets of conditions [Fig. 2.5A(a–c)].

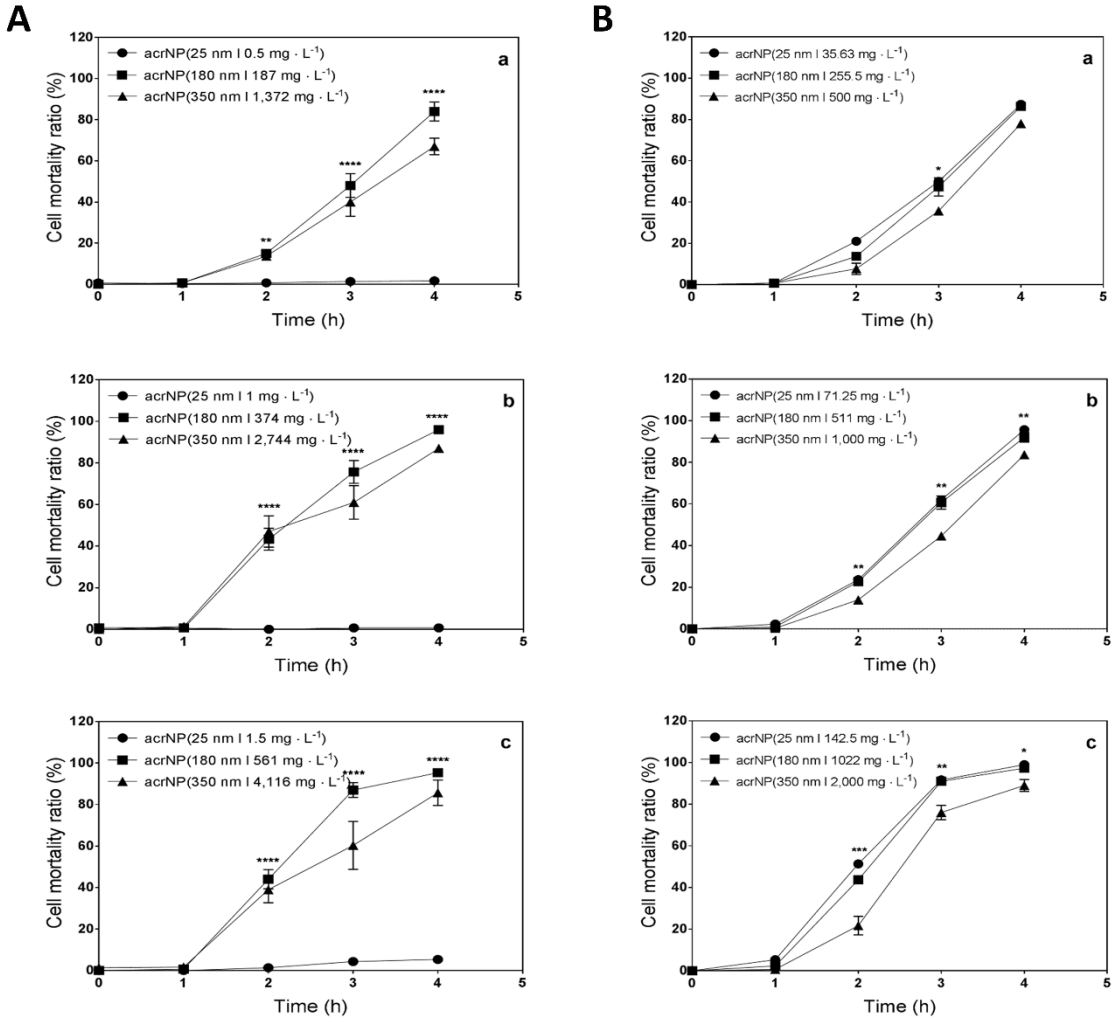

Fig. 2.5 Comparison of cell mortality ratios in wild-type *Chlamydomonas reinhardtii* cells following exposure to three different sized acrylic resin nanoparticles (acrNPs). Cell mortality ratios are shown following exposure to three different sized acrNPs (25 nm, 180 nm, and 350 nm in diameter) (A) under the same molar concentration with three different sets of conditions (a–c) and (B) under the same total surface area with three different sets of conditions (a–c) (see Materials and methods for details on the conditions). Cell mortality ratios were calculated as the number of trypan blue stained and lysed cells observed out of 100 total cells. Results are shown as the mean ratios (±SE) from three independent experiments. Asterisks denote significant differences between treatments at a given time (one-way analysis of variance, * $p < 0.05$, ** $p < 0.01$, *** $p < 0.001$, **** $p < 0.0001$).

For all three sets of conditions in which a constant surface area was used independent of particle size, we found that acrNP(25 nm) and acrNP(180 nm) had essentially identical cell mortality profiles (Pearson's correlation, r = 0.986–1.000) regardless of the acrNP particle size or zeta potential [Fig. 2.5B(a–c), Table 2.3]. By contrast, acrNP(350 nm) had a subtly smaller cell mortality ratio than acrNP(25 nm) and acrNP(180 nm) after 2 hours' exposure.

2.3.7 TEM observation of acrNP exposed wild-type cells

TEM observation of wild-type *C. reinhardtii* cells that had been co-incubated with acrNP(25 nm|65 mg · L^{-1}) for 15 minutes showed that several of the cell wall layers had peeled off (Fig. 2.6) and many acrNP particles had accumulated at the interface between the cell wall and plasma membrane (hereafter, the periplasmic space). Furthermore, these particles were surrounded by a membrane-like structure of uncertain origin (Fig. 2.6). It is worth noting that each membrane-like structure contained at least 5–30 particles, suggesting that they formed following the accumulation of acrNPs in the periplasmic space. In addition, acrNP(25 nm) particles surrounded by a large vesicle were also observed in the cytosol.

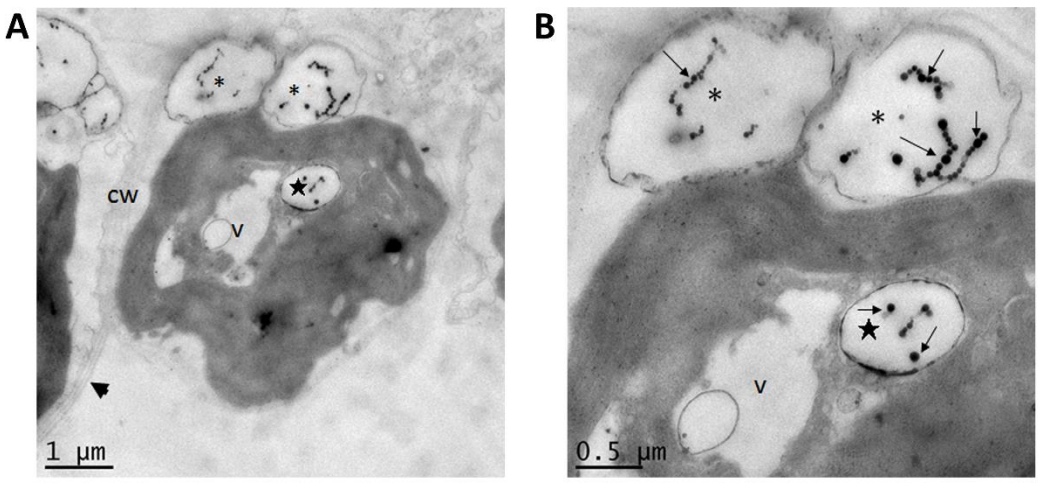

Fig. 2.6 Transmission electron microscope images of a wild-type *Chlamydomonas reinhardtii* cell following exposure to acrylic resin nanoparticles (acrNPs). Cells were exposed to acrNP(25 nm) at a concentration of 65 mg · L^{-1} for 15 minutes and are shown at magnifications of (A) ×2,500 and (B) ×5,000. Each structure (*) with a membrane of unknown origin contained 5–30 acrNP particles (shown by arrows). Two to five of these structures were detected in each cell within the space between the cell wall and the plasma membrane, and some were located in the cytosol (★). The arrowhead in (A) shows the damaged part of the cell wall. CW: cell wall; V: vacuole.

2.3.8 Relationship between the ROS level and cell mortality ratio

We detected a clear, time-dependent increase in DCF fluorescence over the first 2 hours of exposure to acrNP(25 nm|100 mg · L^{-1}) (Fig. 2.7A). The fluorescence peaked at 2 hours, when it was approximately nine times higher than in the untreated control, and then decreased during further incubation. A peak in green DCF fluorescence at 2 hours was also confirmed by microscopic observation (Fig. 2.7C). By contrast, no ROS were generated after 3 hours' exposure to PS-NP(50 nm|100 mg · L^{-1}), TiO_2-NP(100 mg · L^{-1}), or ZnO-NP(100 mg · L^{-1}) (Fig. 2.7A,C). The cell mortality ratio reached 95% after 3 hours' exposure to acrNP(25 nm|100 mg · L^{-1}), whereas neither PS-NP(50 nm|100 mg · L^{-1}), TiO_2-NP(100 mg · L^{-1}) nor ZnO-NP(100 mg · L^{-1}) induced apparent cell death after the same period of exposure (Fig. 2.8A).

We found that cells that were cultured and treated under constant light had significantly higher levels of DCF fluorescence than cells that were cultured and treated in the dark (Fig. 2.7B,D). DCF fluorescence peaked after 2 hours' exposure to acrNP(25 nm|100 mg · L^{-1}) in cells cultured under constant light, at which time the level of fluorescence was approximately nine times as high as in the untreated control and the cell mortality ratio was 89%. By contrast, peak fluorescence occurred after 3 hours of exposure for cells that were cultured and treated in the dark, at which time the level was

only approximately twice as high as in the control and the cell mortality ratio was 32% (Fig. 2.8B).

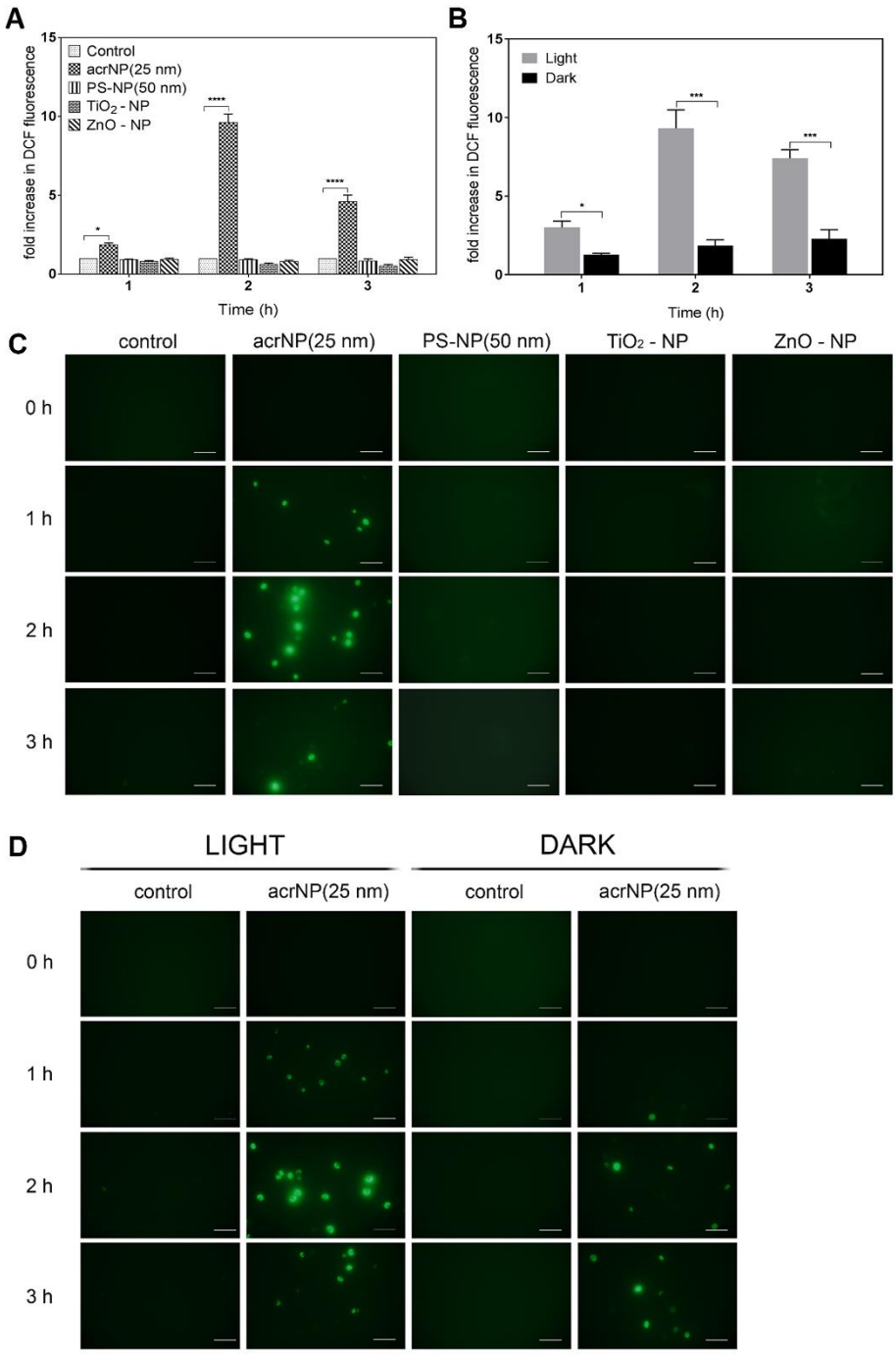

Fig. 2.7. Increase in 2',7'-dichlorofluorescein (DCF) fluorescence in wild-type *Chlamydomonas reinhardtii* cells following exposure to nanoparticles (NPs). The DCF fluorescence intensity was measured using a fluorescence spectrometer to estimate the induced reactive oxygen species (ROS) levels in cells exposed to (A) acrylic resin nanoparticles [acrNP(25 nm)],

polystyrene nanoparticles [PS-NP(50 nm)], or metal oxide nanoparticles (TiO_2-NP and ZnO-NP) at concentrations of 100 mg · L^{-1}; and (B) acrNP(25 nm) at a concentration of 100 mg · L^{-1} under constant light or dark conditions. DCF fluorescence was also observed using a fluorescence microscope, whereby (C) is the representative image for (A) and (D) is the representative image for (B) (bar = 50 μm). In (A) and (B), results are shown as mean ratios (± SE) from three independent experiments and asterisks denote significant differences between the NP treatment and untreated control (A) or the light and dark conditions (B) at a given time (t-test, * $p < 0.05$, ** $p < 0.01$, **** $p < 0.0001$).

No agglomeration between *C. reinhardtii* cells and acrNP(25 nm|100 mg · L^{-1}) was observed even after 3 hours' exposure. By contrast, PS-NP(50 nm), TiO_2-NP(100 mg · L^{-1}), and ZnO-NP(100 mg · L^{-1}) frequently generated agglomerates composed of algal cells and NPs (Fig. 2.9).

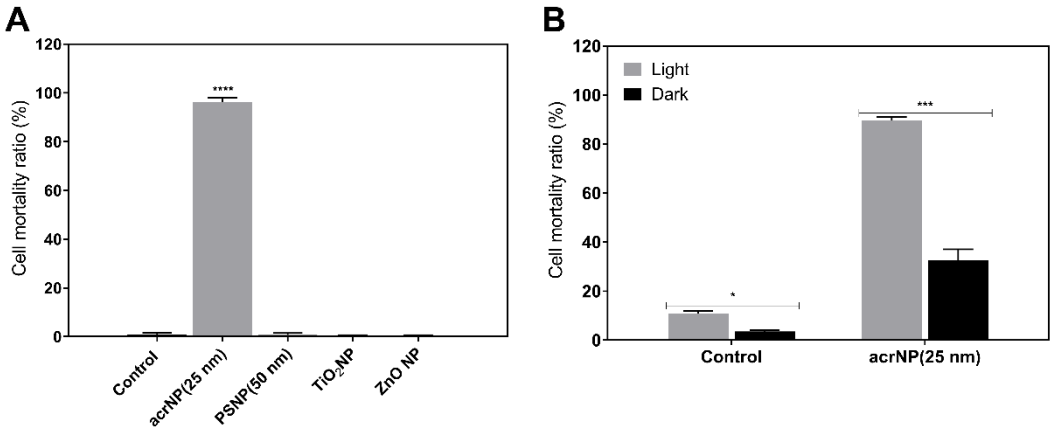

Fig. 2.8. Cell mortality ratios in wild-type *Chlamydomonas reinhardtii* cells following exposure to various nanoparticles and the effect of light conditions. Cells were exposed to (A) acrylic resin nanoparticles [acrNP(25 nm)], polystyrene nanoparticles [PS-NP(50 nm)], or metal oxide nanoparticles (TiO_2-NP and ZnO-NP) at a concentration of 100 mg · L^{-1}; and (B) acrNP(25 nm) at a concentration of 100 mg · L^{-1} under constant light or dark conditions for 3 hours. Cell mortality ratios were calculated as the number of trypan blue stained and lysed cells observed out of 100 total cells. Results are shown as mean ratios (± SE) from three independent experiments. Asterisks denote significant differences between the light and dark at a given time (t-test, * $p < 0.05$, *** $p < 0.001$, **** $p < 0.0001$).

2.3.9 Screening of acrNP-sensitive species in Chlorophyceae

We found that acrNP(25 nm|1,000 mg · L^{-1}|4 h) was sufficient to induce prominent cell mortality of >80% in 20 of the 26 species investigated from the class Chlorophyceae (Table 2.2). By contrast, this treatment induced <5% cell mortality in the remaining six species, which included two species belonging to Sphaeropleales (*Pseudokirchneriella subcapitata* and *Scenedesmus obliquus*) and four species belonging to Volvocales (*Carteria crucifera*, *Chlamydomonas assymetrica*, *Chloromonas actinochloris*, and *Haematococcus lacustris*).

No cell mortality was induced by acrNP(25 nm|1,000 mg · L^{-1}|4 h) in *Euglena gracilis* in the class Euglenophyceae and four species belonging to the class Trebouxiohyceae (*Chlorella sorokiniana*, *Chlorella vulgaris*, *Chloroidium saccharophilum, and Pseudochlorella pringsheimii*).

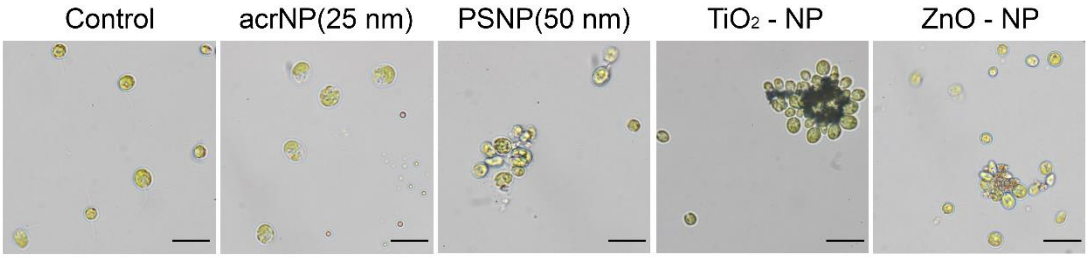

Fig. 2.9 Bright field microscopic observation of wild-type *Chlamydomonas reinhardtii* cells following exposure to various nanoparticles. Cells were exposed to acrylic resin nanoparticles [acrNP(25 nm)], polystyrene nanoparticles [PS-NP(50 nm)], or metal oxide nanoparticles (TiO_2-NP and ZnO-NP) at a concentration of 100 mg · L^{-1} for 30 minutes. Cell–NP agglomerates were observed in the PS-NP(50 nm), TiO_2-NP, and ZnO-NP treatments. (bar = 50 μm)

2.4 Discussion

2.4.1 Acute induction of abnormal swimming

The first abnormal phenomenon we observed in *C. reinhardtii* following exposure to acrNPs was an unusual swimming orbit that included frequent and abrupt directional changes (Video 2.1). It is well known that exposure of *Chlamydomonas* spp. to acids (e.g., acetic acid) causes the flagella to be disconnected immediately [20]. However, most of the acrNP-exposed wild-type cells maintained their flagella, even after they had stopped swimming (Video 2.1), suggesting that some other mechanism was involved.

Using dark field microscopy, we observed that acrNP(180 nm) particles collided with cells in a random and capricious way but no particles became stably entrapped on the cell surface. Thus, this simple collision, which must be the first event that occurs after adding acrNPs to the cell culture, appears to be the first trigger for inducing abnormal physiological cell responses that eventually lead to cell mortality.

Interestingly, *C. reinhardtii* did not seem to swim away from the acrNP(180 nm|100 mg · L^{-1}) particles, the molar concentration of which is unknown. Mitzel et al. [21] previously reported that *Chlamydomonas* show avoidance behavior toward sulfated polystyrene latex (22 nm) at a concentration of $>3 \times 10^{10}$ particles · mL^{-1}. Therefore, it seems that collision effect of acrNP(180 nm|100 mg · L^{-1}) was not sufficiently strong to induce mechanotransduction for avoidance behavior. It has also been shown that the change in cellular redox poise is a key factor for determining swimming direction in *C. reinhardtii*, with cells clearly changing their swimming direction following the addition of ROS or their quencher by switching between positive and negative phototaxis [22-23].

2.4.2 Secretion of cell wall hydrolytic enzyme

Following the abnormal swimming behavior, we clearly observed the cells becoming swollen (Video 2.2). Furthermore, TEM images revealed an apparent

thinning of the cell wall following exposure to acrNP(25 nm|65 mg · L^{-1}|15 min) (Fig. 2.6: arrowhead). This must have been caused by the uncontrolled secretion of cell wall lytic enzyme(s) stored in the periplasmic space rather than newly synthesized enzymes since these spherical and swollen cells started to appear only 20–30 minutes after exposure (Video 2.2).

This lytic activity may have been caused by gametolysin (gamete lytic enzyme, which is a product of the *MMP1* gene), which is stored in an inactive form even in vegetative cells [24-27]. However, further investigation using specific antibodies to gametolysin are required to confirm this.

2.4.3 Effect of the cell wall on sensitivity to acrNP

The intact cell walls of plants and green algae are expected to have pores that are much smaller than the acrNPs used in the present study (i.e., 1–5 nm vs. 25–350 nm) [28-31]. Therefore, almost of all the acrNPs used here could have crossed an intact cell wall to reach the plasma membrane. The acrNP particles reached the plasma membrane of CC-400 immediately after exposure because this strain lacks a cell wall. Since the plasma membrane contains many different kinds of proteins, the acrNP particles will have easily found proteins that they could adsorb, which may have triggered multiple injurious responses that eventually led to cell death. By contrast, the induction of cell mortality was delayed in strains CC-503 and CC-124 due to the presence of a thin or complete cell wall, respectively (Fig. 2.4).

2.4.4 Potency of different NPs for inducing ROS and cell mortality

We found that the surface area of the particles plays a crucial role in the interaction between acrNPs and cells. Thus, it is very reasonable to assume that the greater potency

of acrNP(25 nm) than acrNP(180 nm) or acrNP(350 nm) for inducing cell mortality at a given mass concentration was due to its larger total surface area.

We also found that while exposure to acrNP(25 nm) induced ROS generation and cell mortality very efficiently in wild-type *C. reinhardtii*, exposure to PS-NP(50 nm|100 mg · L^{-1}), TiO_2-NP(100 mg · L^{-1}), or ZnO-NP(100 mg · L^{-1}) did not. These NPs show widely diverse zeta potentials (Table 2.3) but there was no significant relationship between the charge and the level of ROS generation and cell mortality.

Several previous studies have reported that PS-NPs have limited toxic effects on microalgae, such as a reduction in photosynthesis and growth inhibition [12-13], which matches our finding that only low ROS levels were generated. Similarly, it has been reported that TiO_2-NP and ZnO-NP have only limited toxic effects on unicellular green algal species [32-35]. For example, Chen et al. [35] found that TiO_2-NP (anatase and rutile mixture; average particle size, 21 nm) did not have any remarkable toxic effects on cell proliferation in wild-type *C. reinhardtii*. However, they did report that TiO_2-NP particles accumulated on the cell surface following exposure at concentrations of 20 mg · L^{-1} and 100 mg · L^{-1}, and that a limited number of particles penetrated the cell wall, though only a few were located inside the cytoplasm. Similarly, we found that exposure to TiO_2-NP(100 mg · L^{-1}) could induce similar abnormal responses as exposure to acrNPs, though to much less of an extent. Metal oxide NPs also have the potential to induce cell wall lytic enzyme(s), though again to a much more limited extent than acrNPs.

In this study, we demonstrated that exposure of *C. reinhardtii* to acrNPs induces abnormal swimming and cell lysis in the absence of the stable adsorption of particles on the cell wall. However, we did not detect any cell–acrNP agglomerates, despite previous claims that it is these agglomerates that cause oxidative stress and toxicity. Some

studies have similarly argued that the adsorption of non-metal oxide NPs such as PS-NPs and CNTs on the cell wall or the formation of agglomerates with the cells play an important role in inducing cell abnormality through inhibition of the smooth exchange of substances (e.g., oxygen, carbon dioxide, and nutrients) with the external milieu [10,13,36]. However, these were not the first trigger for the process that finally led to cell mortality in *C. reinhardtii* by the exposure of acrNPs.

Toxicity as a result of exposure to metal oxide NPs is known to be caused by solubilized ions and the NPs [6, 34, 37]. For example, the primal toxic effect of ZnO-NPs on *Pseudokirchneriella subscapitata* have been shown to be caused by solubilized Zn^{2+} ions, the release of which is affected by the pH of the medium and the formation of cell–NP agglomerates [33-34].

We also found that the accumulation of ROS following exposure to acrNP(25 nm) was significantly faster in cells that had been cultured and treated under light conditions. This result is in accordance with the findings of a previous study in which *C. reinhardtii* cells were treated with Cd(II) under light and quasi-dark conditions and a lack of light clearly induced a delay in the overproduction of H_2O_2 (Suarez et al. 2013). It has been suggested that light-dependent ROS are mainly produced in the thylakoid membrane by light-driven electron extraction from the oxygen-evolving complex [38-40].

2.4.5 Hypothesized mechanism of acrNP-induced cell mortality

Among the three *C. reinhardtii* strains that were analyzed in this study, cell mortality was most rapidly induced in CC-400. This can only have been due to the lack of a cell wall in this strain, which will have allowed acrNP particles to reach the plasma membrane without needing to wait for the cell wall to be damaged. By contrast, damage

to the cell wall will have been essential for acrNP particles to reach the plasma membrane in strains CC-124 and CC-503 because the pores in the intact cell walls of algae are expected to be much smaller [29-30] than the acrNPs that were used in this study. Consequently, cell mortality was delayed in CC-124 and CC-503.

Once the acrNP particles reach the plasma membrane, they will readily find proteins to which they can stably attach. The stable attachment of the particles seems to be followed by loss of the protein function and also their internalization into the cytosol by some unknown mechanism, which must cause various disorders that lead to high levels of ROS generation.

In those cells that do possess a cell wall, it is most likely that the random collision of acrNPs with the cells inactivates extracellular enzymes (e.g., hydrolytic enzymes that are important for essential nutrient cycling such as β-glucosidase and alkaline phosphatase) and integral proteins that are located on the cell wall, inducing the uncontrolled secretion of hydrolytic enzymes, which causes partial hydrolysis of the cell wall. These extracellular enzymes are essential for nutrient acquisition in aquatic microorganisms [41-43]. Supporting this, Schug et al. [44] showed that exposure of heterotrophic biofilms of a microbial community to TiO_2-NP reduced the activity of extracellular enzymes (such as β-glucosidase and L-leucine aminopeptidase), with the magnitude of this effect depending on the particle coatings. Moreover, it has been postulated that the activity loss of alkaline phosphatase by adsorption to Ag-NPs cause toxic effects in *Euglena gracillis* [36, 45].

We also believe that acrNPs may have a selective interaction with some biomolecules (e.g., enzymes, sensory proteins), whereby they tear them off the cell wall, causing the abnormal reactions that were observed in *C. reinhardtii*. Indeed, cell wall-modifying enzymes, transport/binding proteins, and proteins that are involved in

cell motility have been identified in proteins extracted from the cell wall of the unicellular green alga *Haematococcus pluvialis* [46], which is very closely related to *C. reinhardtii*. In addition, recent studies have shown that latex NPs are able to bind to proteins contained in serum with an apparent specificity that is based on the functional groups on the surface, and a reduction in enzyme activity following adsorption to NPs has also been indicated [47-50].

Interestingly, around one-third of the green algae we examined from the class Chlorophyceae were resistant to acrNP exposure (Table 2.2). According to the above protein deprivation hypothesis, this may be because these species do not have proteins that can interact with acrNPs on their cell walls and so contact with acrNPs cannot induce the secretion of cell wall lytic enzyme(s), preventing the particles from crossing the cell wall.

In this study, we found that high levels of ROS generation occurred in cells that were grown in the light but not in the dark, indicating that photosynthetically active chloroplasts can be one of the predominant sources of ROS (Fig. 2.7B,D), the overproduction of which will eventually lead to cell death. This would also explain why overgrown cells, which have inactive chloroplasts, are relatively insensitive to acrNP exposure.

The series of responses that began with abnormal swimming and ended with cell death is illustrated in Fig. 2.10. Currently, very little is known about how NPs interact with biomolecules, and how their orientation is governed by their size, shape, and surface chemistry. Therefore, analysis of the NP–protein complexes that result from random collision will be essential for uncovering the fundamental mechanisms that are involved.

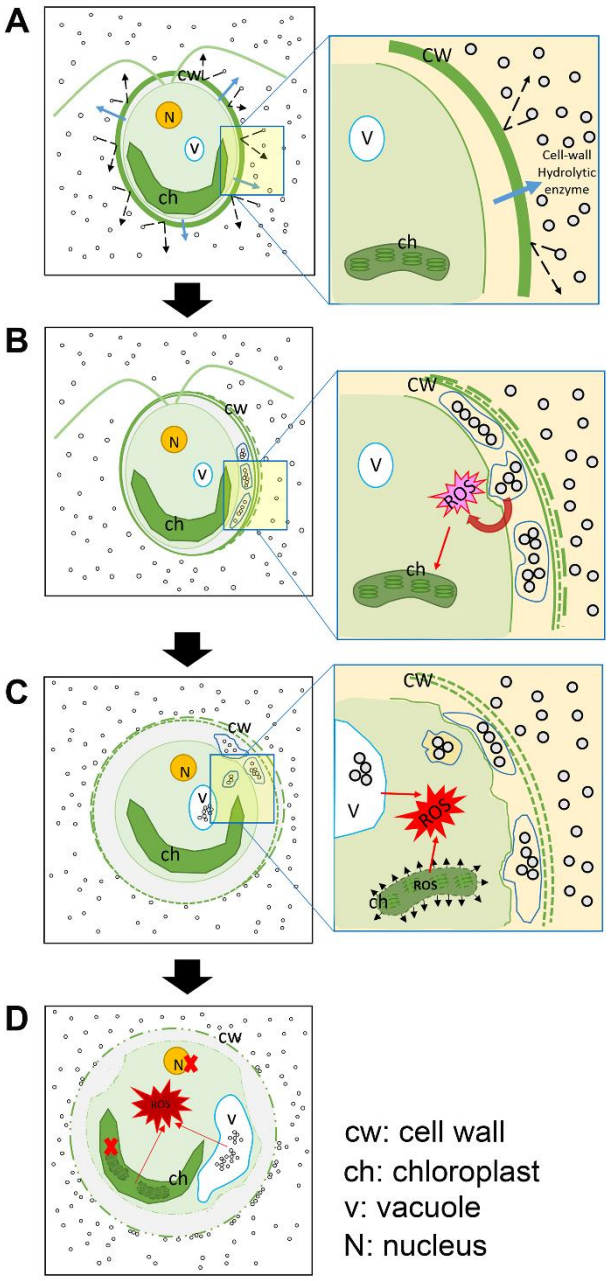

Fig. 2.10 Schematic diagram showing the hypothesized mechanism for acrylic resin nanoparticle (acrNP)-induced cell mortality in *Chlamydomonas reinhardtii*. (A) Random collisions of acrNPs induce the secretion of hydrolytic enzyme(s) stored in the cell. (B) acrNPs pass through the damaged cell wall (broken lines) and then attach to the plasma membrane, where they are enveloped by a membrane of unknown origin. The generation of primary reactive oxygen species (ROS) is induced by this collision and the direct attachment of acrNPs on the plasma membrane. (C) acrNPs are internalized into the cytosol through an endocytosis-like mechanism, which is accompanied by damage to organelles, such as plastids, generating a much larger amount of ROS. (D) The accumulation of high levels of ROS and the severe damage these cause to proteins and membranes eventually lead to cell death.

2.5 References

1. Navarro, E., Baun, A., Behra, R., Hartmann, N.B., Filser, J., Miao, A.J., Quigg, A., Santchi, P.H. & Sigg, L. 2008. Environmental behavior and ecotoxicity of engineered nanoparticles to algae, plants, and fungi. *Ecotoxicology*. 17(5): 372-386.
2. Maurer-Jones, M.A., Gunsolus, I.L., Murphy, C.J. & Haynes, C.L. 2013. Toxicity of engineered nanoparticles in the environment. *Anal. Chem*. 85(6): 3036-3049.
3. Bhatia, S. 2016. *Natural Polymer and Delivery System: Nanoparticles, Plants, and Algae*. Springer international publishing, Switzerland, pp. 33-93.
4. Nel, A., Xia, T., Madler, L. & Li, N. 2006. Toxic potential of materials at the nanolevel. *Science*. 311(5761): 622-627.
5. Yu, E., Pavlov, D.S., Demidova, T.B. & Dgebuadze, Y.Y. 2010. Effect of nanoparticles on aquatic organisms. *Biol. Bull. Russ. Acad. Sci*. 37(4): 406-412.
6. Quigg, A., Chin, W., Chen, C., Zhang, S., Jiang, Y., Miao, A., Schwehrll, K.A. & Santschi, P.H. 2013. Direct and indirect toxic effect of engineered nanoparticles on Algae: Role of natural organic matter. *ACS Sustainable Chem. Eng*. 1(7): 686-702.
7. Miazek, K., Iwanek, W., Remacle, C., Richel, A. & Goffin, D. 2015. Effect of metals, metalloids, and metallic nanoparticles on microalgae growth and industrial product biosynthesis: a review. *Int. J. Mol. Sci.* 16(10): 23929-23969.
8. Libralato, G., Galdiero, E., Falanga, A., Carotenuto, R., de Alteriis, E. & Guida, M. 2017. Toxicity effects of functionalized Quantum Dots, gold, and polystyrene nanoparticles on target biological models: A review. *Molecules*. 22: 1439.

9. Basiuk, E.V., Ochoa-Olmos, O.E. & De la Mora-Estrada, L.F. 2011. Ecotoxicological effects of carbon nanomaterials on algae, fungi, and plants. *J. Nanosci. Nanotechnol.* 11(4): 3016-3038.
10. Schwab, F., Bucheli, T.D., Lukhele, L.P., Magrez, A., Nowack, B., Sigg, L. & Knauer, K. 2011. Are carbon nanotube effects on green algae caused by shading and agglomeration? *Environ. Sci. Technol*. 45: 6136-6144.
11. Sohn, E.K., Chung, Y.S., Johari, S.A., Kim, T.G., Kim, J.K., Lee, J.H., Lee, Y.H., Kang, S.W. & Yu, I.J. 2015. Acute toxicity comparison of single-walled carbon nanotubes in various freshwater organisms. *BioMed Res. Int*. Article ID 323090. http://dx.doi.org/10.1155/2015/323090.
12. Bhattacharya, P., Lin, S., Turner, J.P. & Ke, P.C. Physical Adsorption of Charged Plastic Nanoparticles Affects Algal Photosynthesis. 2010. *J. Phys. Chem.: C*. 114: 16556-16561.
13. Nolte, T.M., Hartmaan, N.B., Klejin, J.M., Garnæs, J., van de Meent, D., Hendriks, A.J. & Baun, A. 2017. The toxicity of plastic nanoparticles to green algae as influenced by surface modification, medium hardness and cellular adsorption. *Aquat. Toxicol*. 183: 11-20.
14. Vauthier, C., Dubernet, C., Fattal, E., Pinto-Alphandary, H. & Couvreur, P. 2003. Poly(alkylcyanoacrylates) as biodegradable materials for biomedical applications. 2003. *Adv. Drug Deliv. Rev.* 55: 519–548.
15. Sulheim, E., Baghirov, H., Haartman, E.V., Bøe, A., Aslund, A.K.O., Mørch, Y. & de Lange Davis, C. 2016. Cellular uptake and intracellular degradation of poly(alkyl cyanoacrylate) nanoparticles. *J. Nanobiotechnology*. **14**:1 https://doi.org/10.1186/s12951-015-0156-7

16. Shirotake, S. 2014. A new cyanoacrylate colloidal polymer with novel antibacterial mechanism and its application to infection control. *J Nanomedine Biotherapeutic Discov.* 4(1): 1-7. DOI:10.4172/2155-983X.1000122

17. Hyams, J. & Davies, D. 1972. Induction and characterization of cell wall mutants of *Chlamydomonas reinhardtii*. *Mutat. Res*. 14(4): 381-389.

18. Fuentes, C. & Vanwinkle-swift, K. 2003. Isolation and characterization of a cell wall-defective mutant of *Chlamydomonas monoica* (Chlorophyta). *J. Phycol*. 39(6): 1261-1267.

19. Gorman, D.S. & Levine, R.P. 1965. Cytochrome f and plastocyanin: their sequence in the photosynthetic electron transport chain of *Chlamydomonas reinhardi*. *Proc. Natl. Acad. Sci. USA*. 54(6): 1665-1669.

20. Craige, B., Brown, J. & Witman, G. 2013. Isolation of *Chlamydomonas* flagella. *Curr Protoc Cell Biol*. 59(3): 3.41-3.41.9. DOI: 10.1002/0471143030.cb0341s59.

21. Mitzel, M.R., Lin, N., Whalen, J.K. & Tufenkii, N. 2017. *Chlamydomonas reinhardtii* displays aversive swimming response to silver nanoparticles. *Environ. Sci.: Nano*. 4: 1328-1338.

22. Wakabayashi, K. & King, S.M. 2006. Modulation of *Chlamydomonas reinhardtii* flagellar motility by redox poise. *J. Cell. Biol*. 173(5): 743-754. DOI: 10.1083/jcb.200603019

23. Wakabayashi, K., Misawa, Y., Mochiji, S. & Kamiya, R. 2011. Reduction-oxidation poise regulates the sign of phototaxis in *Chlamydomonas reinhardtii*. *Proc. Natl. Acad. Sci. USA*. 108(27): 11280-11284.

24. Matsuda, Y., Saito, T., Yamaguchi, T., Koseki, M. & Hayashi, K. 1987. Topography of cell wall lytic enzyme in *Chlamydomonas reinhardtii*: form and

location of the stored enzyme in vegetative cell and gamete. *J. Cell. Biol*. 104: 321-329.

25. Buchanan, M.J., Imam, S.H., Eskue, W.A. & Snell, W.J. 1989. Activation of the cell wall degrading protease, lysin, during sexual signaling in *Chlamydomonas*: the enzyme is stored as an inactive, higher relative molecular mass precursor in the periplasm. *J. Cell. Biol.* 108: 199-207.
26. Kinoshita, T., Fukuzawa, H., Shimada, T., Saito, T. & Matsuda, Y. 1992. Primary structure and expression of a gamete lytic enzyme in *Chlamydomonas reinhardtii*: similarity of functional domains to matrix metalloproteases. *Proc. Natl. Acad. Sci. USA*. 89(10): 4693-4697.
27. Kubo, T., Saito, T., Fukuzawa, H. & Matsuda, Y. 2001. Two tandemly-located matrix metalloprotease genes with different expression in the *Chlamydomonas* life cycle. *Curr. Genet*. 40: 136-137.
28. Carpita, N., Sabularse, D., Montezinos, D. & Delmer, D. 1979. Determination of the pore size of cell walls of living plants cells. *Science.* 205(4411): 1144-1147.
29. Demchick, P. & Koch, A.L. 1996. The permeability of the wall fabric of *Escherichia coli* and *Bacillus subtilis*. *J Bacteriol*. 178(3): 768-773.
30. Berestovsky, G.N., Ternovsky, V.I. & Kataev, A.A. 2001. Through pore diameter in the cell wall of *Chara coralina*. *J. Exp. Bot.* 52(359): 1173-1177.
31. Davison, B.H., Parks, J., Davis, M.F. & Donohoe, B.S. 2013. Plant Cell Walls: Basics of Structure, Chemistry, Accessibility and the Influence on Conversion. *In* Wymann, C.E. [Eds]. *Aqueous Pretreatment of Plant Biomass for Biological and Chemical Conversion to Fuels and Chemicals*. John Wiley & Sons Ltd., Chichester, UK, pp. 23-38. DOI: 10.1002/9780470975831.ch3.

32. Hund-Rinke, K. & Simon, M. 2006. Ecotoxic effect on photocatalytic active nanoparticles TiO2 on algae and daphnids. *Environ. Sci. Pollut. Res*. 17(5): 372-386.

33. Franklin, N.M., Rogers, N.J., Apte, S.C., Batley, G.E., Gadd, G.E. & Casey, P.S. 2007. Comparative toxicity of nanoparticulate ZnO, Bulk ZnO, and ZnCl2 to a freshwater microalga (*Pseudokirchnereilla subcapitata*): the importance of particle solubility. *Environ. Sci. Technol*. 41(24): 8484-8490.

34. Aruoja, V., Dubourguier, H.C., Kasemets, K. & Kahru, A. 2009. Toxicity of nanoparticles of CuO, ZnO, and TiO2 to microalgae *Pseudokirchneriella subcapitata*. *Sci. Total Environ*. 407(4): 1461-1468.

35. Chen, P., Powell, B.A., Mortimer, M. & Ke, P.C. 2012. Adaptive interactions between zinc oxide nanoparticles and *Chlorella* sp. *Environ. Sci. Technol.* 46(21): 12178-12185.

36. Li, X. 2015. Interaction of silver and polystyrene nanoparticles with algae. Ph.D. dissertation, École polytechnique fédérale de Lausanne, Lausanne, pp. 41-66. Available at: https://infoscience.epfl.ch/record/213652/files/EPFL_TH6818.pdf

37. Oukarroum, A., Zaidi, W., Samadani, M., & Dewez, D. 2017. Toxicity of nickel oxide nanoparticles on a freshwater green algal strain of *Chlorella vulgaris*. *BioMed Res. Int*. Article ID: 9528180. https://doi.org/10.1155/2017/9528180

38. Asada, K. 2006. Production and scavenging of reactive oxygen species in chloroplast and their function. *Plant Physiol*. 141(2): 391-396.

39. Suarez, G., Santschi, C., Slaveykova, V.I. & Martin, O.J.F. 2013. Sensing the dynamics of oxidative stress using enhanced absorption in protein-loaded random media. *Sci. Rep*. 3(3447): 1- 8.

40. Propíšil, P. 2016. Production of Reactive Oxygen Species by photosystem II as a response to light and temperature. *Front. Plant Sci*. 7: 1950.

41. Zaccone, R & Caruso, G. 2002. Microbial hydrolysis of polysaccharides and organic phosphates in the Nothern Adriatic Sea. *Chem. Ecol*. 18:85-94.

42. Hoppe, H.G. 2003. Phosphatase activity in the sea. *Hydrobiologia*. 493: 187-200

43. Caruso, G. 2010. Leucine aminopeptidase, beta-glucosidase and alkaline phosphatase activity rates and their significance in nutrient cycles in some coastal Mediterranean sites. *Mar. Drugs*. 8(4): 916-940.

44. Schug, H., Isaacson, C.W., Sigg, L., Amman, A.A. & Schirmer, K. 2014. Effect of TiO2 nanoparticles and UV radiation on extracellular enzyme activity of intact heterotophic biofilms. *Environ. Sci. Technol*. 48(19): 11620-11628.

45. Yue, Y., Li, X., Sigg, L., Suter, M.J., Pillai, S., Behra, R. & Schirmer, K. 2017. Interaction of silver nanoparticles with algae and fish cells: a side by side comparison. *J. Nanobiotechnology*. 15:16.

46. Wang, S.B., Hu, Q., Sommerfield, M., & Chen, F. 2004. Cell wall proteomics of the green algae *Haematococcus pluvialis* (Chlorophyceae). *Proteomics*. 4(3): 692-708.

47. Gessner, A., Lieske, A., Paulke, B.R. & Muller, R.H. 2003. Functional groups on polystyrene nanoparticles: influence the protein adsorption. *J. Biomed Mater. Res. A*. 65(3): 319-326

48. Lundqvist, M., Stigler, J., Elia, G., Lynch, I., Cedervall, T. & Dawson, K.A. 2008. Nanoparticle size and surface properties determine the protein corona with possible implications for biological impacts. *Proc. Natl. Acad. Sci. USA*. 105(38): 14265-14270.

49. Saptarshi, S.R., Duschl, A. & Lopata, A.L. 2013. Interaction of nanoparticles with proteins: relation to bio-reactivity of the nanoparticle. *J. Nanobiotechnology*. 11: 26.

50. Sun, X., Feng, Z., Zhang, L., Hou, T. & Li, Y. 2014. The selective interaction between silica nanoparticles and enzymes from molecular dynamic simulations. *Plos One*. 9(9): e107696. https://doi.org/10.1371/journal.pone.0107696

CHAPTER 3. Rapid protoplast generation of *Chlorella vulgaris* and related species after exposed to acrylic resin nanoparticles

3.1 Introduction

Resin nanoparticles made of cyanoacrylate are expected to be a promising material for drug delivery [1]. Shirotake [2] unexpectedly found that *n*-butyl-cyanoacrylate nanoparticles induce bacteriolysis in Gram-positive bacteria, but not in Gram-negative bacteria. He [2] proposed that this nanoparticle directly binds to the peptidoglycan layer of Gram-positive bacteria, where they locally inhibit peptidoglycan synthesis at the attachment site, which ultimately induces bacteriolysis.

Also unexpectedly, we found that exposure with the same isobutyl-cyanoacrylate nanoparticles (acrNPs) efficiently induce protoplast-like cells in *Chlorella vulgaris* and *Pseudochlorella pringsheimii*, which are both unicellular green algae species belonging to the Trebouxiophyceae class. Here, we have reported the methods and the possible mechanisms for inducing protoplasts/spheroplast by exposure to acrNPs.

3.2 Materials and Methods

3.2.1 Strains and culture conditions

All algal species shown below were provided by the Microbial Culture Collection at the National Institute for Environmental Studies (NIES-Collection) (Tsukuba, Japan): *P. pringsheimii* NIES-2150, *Chloroidium saccharophilum* NIES-2352 [3], *Chlorella sorokiniana* NIES-2169, and *C. vulgaris* NIES-2170.

All algal species except *C. vulgaris* were cultured in the medium recommended by NIES under constant fluorescent light (84 μmol photons μm^{-2} s^{-1}) with gentle shaking,

whereas *C. vulgaris* was cultured in Tris-acetate-phosphate medium (TAP) (pH 7.0) [4] under the same lighting condition. Cells at the mid-log phase (OD_{750} around 0.8) were used for treatments, unless mentioned otherwise.

3.2.2 Nanoparticles

Three different sized acrNPs (25 nm, 180 nm, and 350 nm in diameter) made of poly(isobutyl-cyanoacrylate) were kindly supplied by CHIKAMI MILTEC INC. (Kochi, Japan). All the supplied-acrNPs were suspended in dispersing reagents as mentioned in detail in section 2.2.1. All of the dispersed diameter values were based on measurements taken immediately after production using the dynamic light scattering (DLS) method. Data sheets were kindly provided by CHIKAMI MILTEC INC. (Table 2.1).

Two types of metal oxide nanoparticles were used in this study. The ZnO particles (544906, Sigma) were less than 100 nm in size. The size of the TiO_2 (anatase form) particles (205-01715, Wako Chem., Japan) is unknown.

3.2.4 Exposure of *C. vulgaris* and related species with acrNPs

To assay the possible cellular lytic effects and protoplast/spheroplast induction by exposure to acrNPs, we exposed the exponentially growing cells with acrNPs of three sizes (25, 180, and 350 nm) and at three concentrations (100 mg • L^{-1}, 250 mg • L^{-1}, and 1000 mg • L^{-1}). Incubations were carried out with very gentle rotation (10 rpm) using 1.5- or 5-mL plastic sample tubes that were placed on their sides in dim light. Negative controls were prepared as exposure with only the dispersants used to prepare acrNPs.

3.2.5 Preparation of protoplasts using commercially available cell-wall lytic enzymes

We used a modified method from Hatano et al. [7] to prepare protoplasts from *C. vulgaris*. A mixture of commercially available lytic enzymes [0.5% Cellulysin (Calbiochem), 2% Macerozyme R-10 (Yakult Pharmaceutical), and 1% chitosanase derived from Bacillus R-4 (K-I Chemical Industry)] in 25 mM phosphate buffer (pH 7.0) with 0.5 M mannitol was used. Cells were harvested at mid-log phase (OD_{750} = 0.8–1.0) by centrifugation (1,000 × *g*, 10 min), and then cell pellets were suspended in the above enzyme mixture (2×10^8 cells • mL^{-1}) and incubated for 4 to 8 h at 25 °C with very gentle shaking in dim light.

3.2.6 Cell-wall-specific staining with Fluorescent Brightener 28

To stain the cell walls containing chitin [5-6], we used Fluorescent Brightener 28 (F3543, Sigma-Aldrich). A stock solution (1 mg • mL^{-1} in H_2O) of the dye was added to the cell culture (final concentration 0.04 mg/mL). Samples were kept in the dark for 10 min preceding the observations. Stained cells were observed without a washing step.

3.2.7 Microscopic observation

Bright-field observations were carried out using an Olympus IX71 (Olympus, Japan), whereas dark-field observations required a specific condenser U-DCD (Olympus, Japan). Fluorescence observations were made using an Olympus IX71 (Olympus, Japan) with a combination of appropriate mirror units.

3.2.8 Assay for cell-wall lytic activity in acrNP-exposed cell culture filtrates

Chlorella vulgaris cells in log-phase growth were harvested by centrifugation (1,000 × *g*, 10 min), and the cell pellet was suspended (1×10^9 cells/mL) in 25 mM phosphate buffer (pH 7.0) containing 0.5 M mannitol and 1 g • L^{-1} of acrNPs(350 nm). After an 8-h coincubation with acrNPs(350 nm) at a concentration of 1 g • L^{-1}, cells were re-harvested by centrifugation (1,000 × *g*, 10 min, 4 °C).

The supernatant was filtered using a Millex-VV syringe filter unit (Merck) with a 100-nm pore diameter to remove remaining acrNPs (350 nm). The filtrate then was used to resuspend the pellet of exponentially grown *C. vulgaris* cells. The cell suspension (2×10^7 cells • mL^{-1}) was incubated in the filtrate for 8 h at 25 °C with very gentle shaking, after which time we looked for evidence of cell-wall lytic activity in the filtrate by checking the generated protoplasts.

3.3 Results and Discussion

3.3.1 Induction of protoplasts

Considering that n-butyl-cyanoacrylate nanoparticle can induce bacteriolysis in various Gram-positive bacteria [2], we exposure *C. vulgaris*, which is a unicellular alga belonging to the Trebouxiophyceae class, with the same type of nanoparticles (acrNP) to see if they would induce algal cell lysis. Three different-sized acrNPs (1 g • L^{-1}) had the potency to generate protoplasts/spheroplasts (Fig. 3.1). Exposure of *Chlorella* cells in exponentially growing phase with acrNP of mean size 180 nm [acrNP(180 nm)] at concentration of 1 g • L^{-1} [hereafter, acrNP(180 nm) (1 g • L^{-1})] for overnight at room temperature unexpectedly resulted in aggregated whole cells at the bottom of the 5-mL sample cup. No cell lysis was observed, suggesting the change at their surface.

We made microscope observations of the acrNP-exposed *Chlorella* cells to see if the cell walls remained intact. The typical cell shape of *C. vulgaris* is spherical, so the

shape itself is not a useful characteristic for distinguishing protoplasts and spheroplasts (protoplasts/spheroplasts) from non-protoplast cells; therefore, we employed a fluorescent dye. Fluorescent Brightener 28 specifically binds to chitin within the cell wall to determine the emergence of protoplasts/spheroplasts [5-6, 8]. In this assay, cells with pure-red fluorescence were judged as protoplasts/spheroplasts, whereas those with pinkish-red fluorescence were evaluated as non-protoplasts/spheroplasts [9-10]. To establish guidelines for this judgement, we prepared protoplasts of *C. vulgaris* using commercially available cell-wall lytic enzymes. The pinkish-red color of nontreated cells was used as a standard for non-protoplasts, which resulted from the overlaid color of pure-red autofluorescence from chlorophylls and blue fluorescence from the Fluorescent Brightener 28 [Fig. 3.1(a)]. The standard reference for protoplasts was generated by introducing cells to the commercially available enzyme mixture for 8 h and then staining with Fluorescent Brightener 28. Owing to the enzyme incubation, the cell walls were stripped-out and, therefore, did not take up the Fluorescent Brightener 28, resulting in pure-red fluorescent cells that were used as a standard reference for protoplasts (Fig. 3.1(b)).

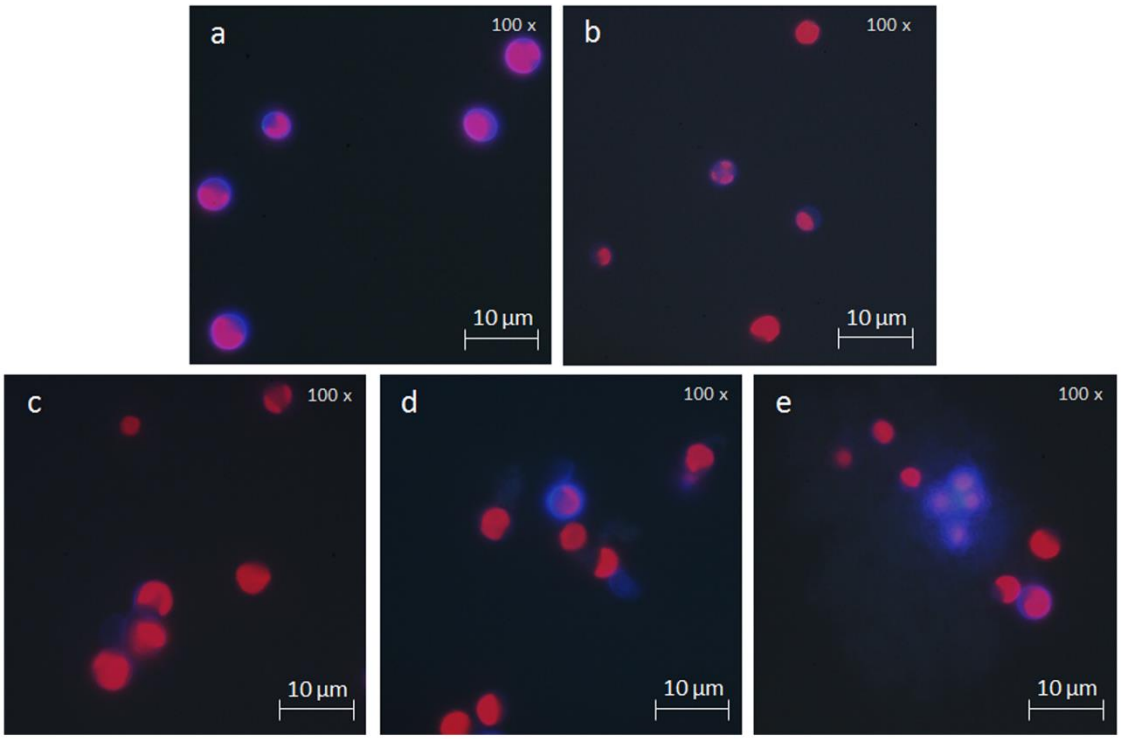

Fig. 3.1 Appearance of protoplasts/spheroplasts after exposure with isobutyl-cyanoacrylate nanoparticles (acrNPs). After exposure, the *Chlorella vulgaris* cell walls were stained with Fluorescent Brightener 28. Untreated cells (a). Protoplast cells generated by a lytic enzyme mixture for 8 h (b). Protoplast-like cells formed after exposed with acrNPs(25 nm) (c), acrNPs(180 nm) (d), and acrNPs(350 nm) (e) for 8 h at a concentration of 1 g • L^{-1}.

We periodically removed subsamples and counted the number of protoplasts/spheroplasts-like cells observed in a total of 100 cells, following the above standard. At the lower acrNP concentration, the peak ratio of protoplasts/spheroplasts was evidently limited, irrespective of acrNP sizes. For example, at a concentration of 250 mg • L^{-1} of acrNPs(25 nm) [Fig. 3.2(a)], the peak ratio of protoplasts/spheroplasts was only ~5%. Otherwise, the peak frequency of protoplasts/spheroplasts reached about 60% after a 4-h coincubation with acrNP(25 nm) (1 g • L^{-1}) [Fig. 3.2(b)]. Slowly decreasing ratios in longer incubations were most likely suggesting a mechanical disruption in the protoplasts/spheroplasts over the generations. It is worth noting that cells in the stationary phase were rather insensitive to acrNP treatment and the

protoplast/spheroplast ratio was limited to about 4% by the same treatment. Regarding the efficiency of protoplast/spheroplast formation, acrNPs(25 nm) (1 g • L^{-1}) were much more efficient than acrNPs(180 nm) (1 g • L^{-1}) and acrNP(350 nm) (1 g • L^{-1}) [Fig. 3.2(b)]. Therefore, to efficiently induce protoplasts/spheroplasts formation, coincubations with acrNPs(25 nm) at high molar concentrations must be a key factor (Fig. 3.2).

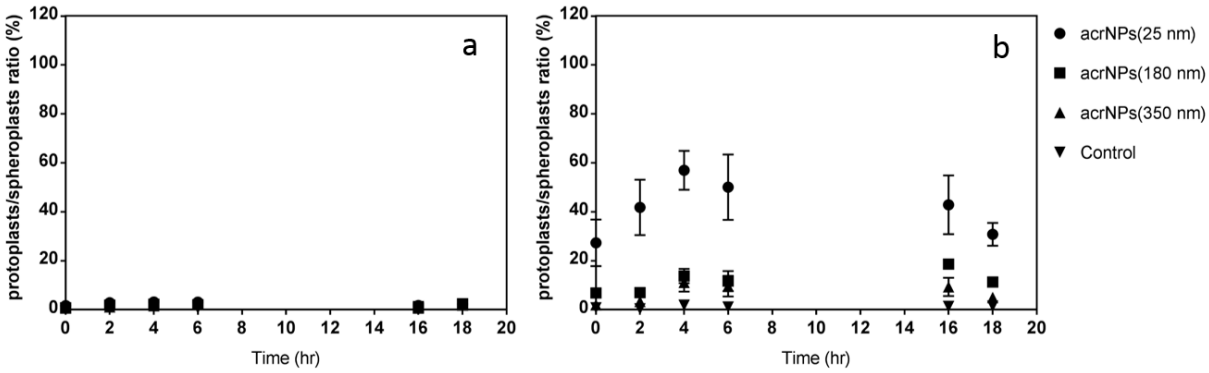

Fig. 3.2 Time course analysis of the protoplast/spheroplast ratio in *Chlorella vulgaris* by coincubation with different-sized isobutyl-cyanoacrylate nanoparticles (acrNPs; 25, 180, and 350 nm in diameter) at a concentration of 250 mg • L^{-1} (a) and 1 g • L^{-1} (b). For the ratio to be determined, the number of pure-red fluorescent cells observed out of 100 total cells was counted. For control, Chlorella cells were coincubated in TAP media without acrNPs. Data shown are mean ± standard error (n = 3).

Using dark-field observation, we were able to directly detect the acrNPs(180 nm) in the culture medium. With these observations, we noticed that acrNPs(180 nm) only collided with the cells in the first hour of exposure (Movie 3.1). In this stage, we rarely detected acrNPs that were attaching stably on the cell surface. However, after the initial hour of the exposure, the number of acrNPs that began to attach securely to the cell surface increased gradually. After 18 h of treatment, four to eight acrNPs were stably binding onto the many exposed cells [Fig. 3.3(a)]. This result coincided with the result obtained after 18 h of exposure with fluorescein isothiocyanate-labeled

acrNPs(180 nm) [Fig. 3.3(b-c)]. The stable attachment of acrNPs to cells probably reflects a change in the cell-wall surface. After a long time exposure to acrNPs, the cell wall is very likely covered with sticky hydrolytes of the cell-wall [11]. The binding of acrNPs to the cell surface was not weak, as after three wash treatments the fluorescein isothiocyanate acrNPs(180 nm) remained attached. Wash treatments included centrifugation at 3,000 × g for 5 min and resuspended in the original volume of the culture medium [Fig. 3.3(b-c)].

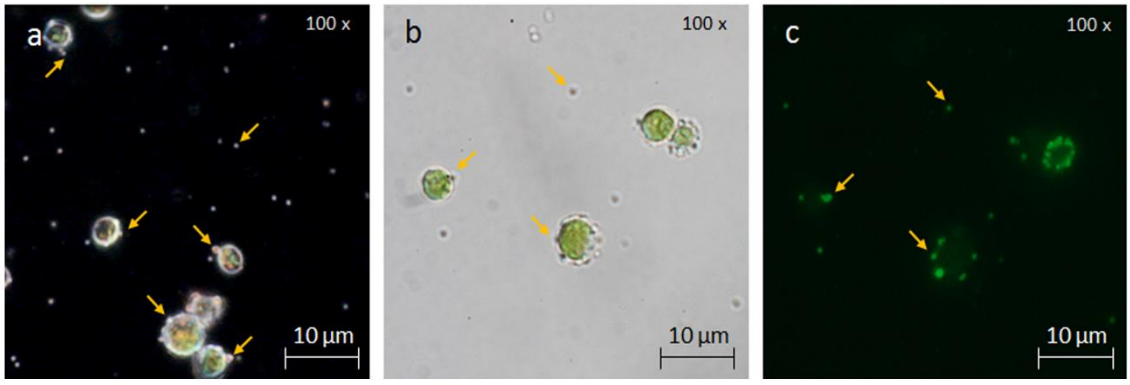

Fig. 3.3 *Chlorella vulgaris* cells that were exposure with isobutyl-cyanoacrylate nanoparticles (acrNPs) (180 nm) (a) or fluorescein isothiocyanate (FITC)-conjugated NPs(180 nm) [(b)–(c)] for 16 h at a concentration of 1 g • L^{-1}. Dark-field microscopy images (a). Light microscopy image (b), and the fluorescence microscopic image of (b) is shown as (c). Arrows indicate the very small homo-aggregates of acrNPs(180 nm) in (a) or FITC-conjugated NPs(180 nm) [(b), (c)].

Exposure cells with only the dispersants used for acrNP(25 nm) preparation (negative controls) were not significantly different from untreated cells. This was also true for the dispersant solutions used for the preparation of acrNP(180 nm) and acrNP(350 nm). Therefore, protoplast/spheroplast induction must be triggered by the actual contact of the acrNPs with the cells.

3.3.2 Secretions confirming cell-wall lytic activity

We confirmed cell-wall lytic activity by secretions detected in the culture medium, as follows. Cells were harvested after an 8-h exposure with acrNP(350 nm, 1 g • L^{-1}), and then the supernatant was filtered using a membrane filter unit with a 100-nm pore size to remove acrNP(350 nm), of which the lower end of the size range was around 150 nm. The filtrate was added to the cell pellet prepared from exponentially grown *C. vulgaris*. After an 8-h incubation in the filtrate containing no acrNPs, about 15% of the cells were changed into protoplasts/spheroplasts (Fig. 3.4). This showed that the filtrate contained abnormally secreted cell-wall lytic enzymes due to acrNP exposure.

3.3.3 Exposure of acrNPs to *C. vulgaris*-related species

We tested to see if a 4-h exposure with acrNPs(25 nm, 1 g • L^{-1}) could induce protoplasts in *C. vulgaris*-related species [3], also belonging to the Trebouxiophyceae class: *P. pringsheimii*, *C. saccharophilum*, and *C. sorokiniana*. In *P. pringsheimii*, protoplasts/spheroplasts were induced at nearly the same level as *C. vulgaris*, whereas in *C. saccharophilum* and *C. sorokiniana*, the protoplasts/spheroplasts generation was not significantly different from that of the nontreated negative control, that is, 3–5% (Fig 3.5). Considering these results, more species should be analyzed to determine which shared biochemical characteristics or phylogenetic classifications render algal species susceptible to acrNPs.

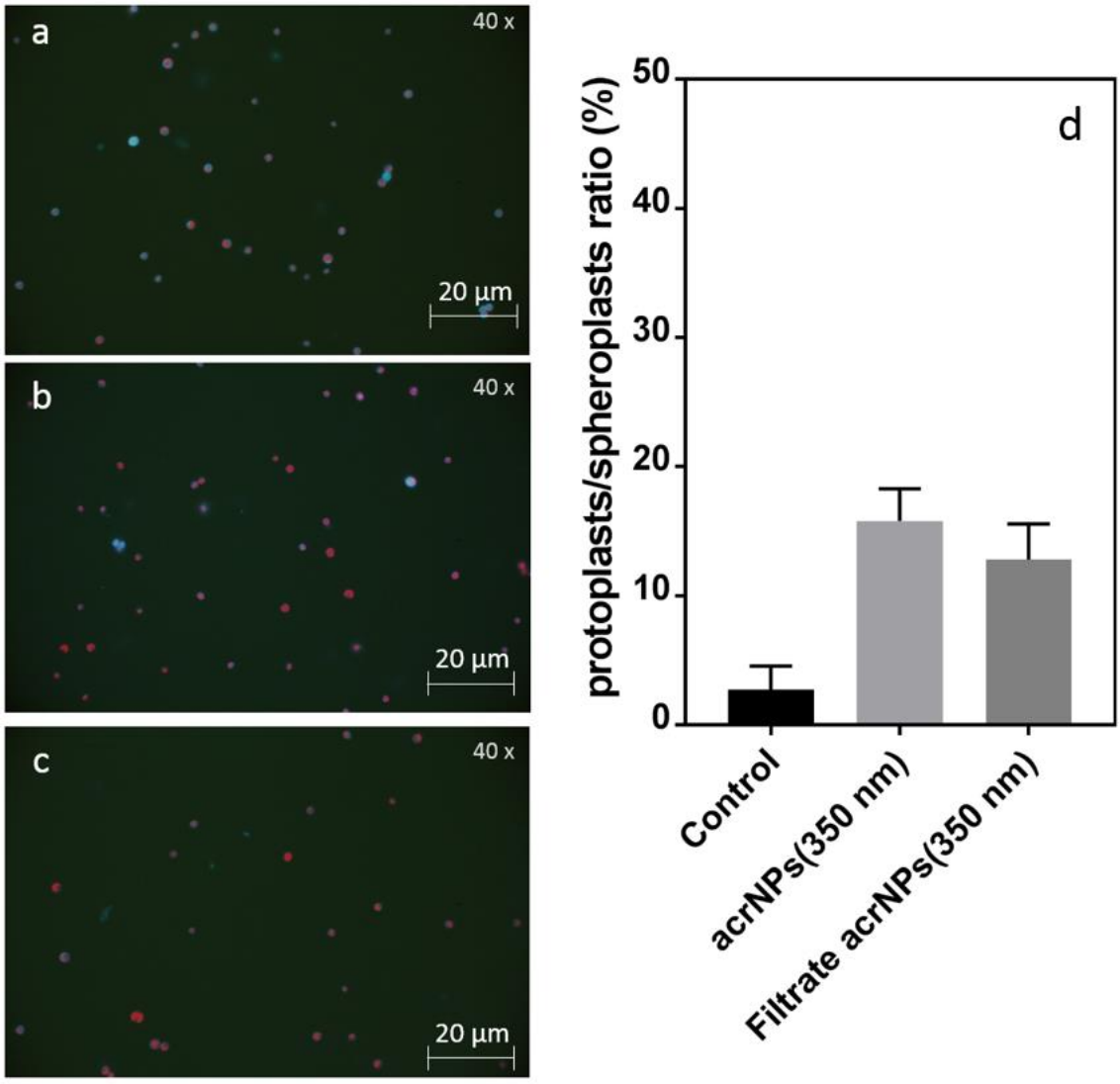

Fig. 3.4 Assay of cell-wall lytic activity contained in the isobutyl-cyanoacrylate nanoparticle (acrNP) coincubation medium. *Chlorella vulgaris* was incubated for 8 h in Tris-acetate-phosphate (TAP) containing acrNP(350 nm) dispersant as a control (a), in TAP containing acrNPs(350 nm) at a concentration of 1 g • L^{-1} (b), and in the filtrate from (b) as shown in (c). *C. vulgaris* cells were stained with Fluorescent Brightener 28 preceding fluorescence microscopy observation. The protoplast/spheroplast ratios detected in (a), (b), and (c) are shown in (d). Data shown are mean ± standard error (n = 3)

3.3.4 Exposure of *C. vulgaris* with metal oxide nanoparticles

In contrast to the efficiency of protoplasts/spheroplasts generated by acrNPs (g • L^{-1}), we could not detect apparent increments of pure-red cells in *C. vulgaris* coincubations with ZnO-NP (1 g • L^{-1}) (4 h) (particles size less than 100 nm) or TiO_2-NP (1 g • L^{-1}) (4 h) (particles size were unknown) (Fig. 3.6). This suggests that acrNPs

had a higher potential than metal oxide nanoparticles to induce cell-wall lytic activity in *C. vulgaris* when the mass concentration was the same.

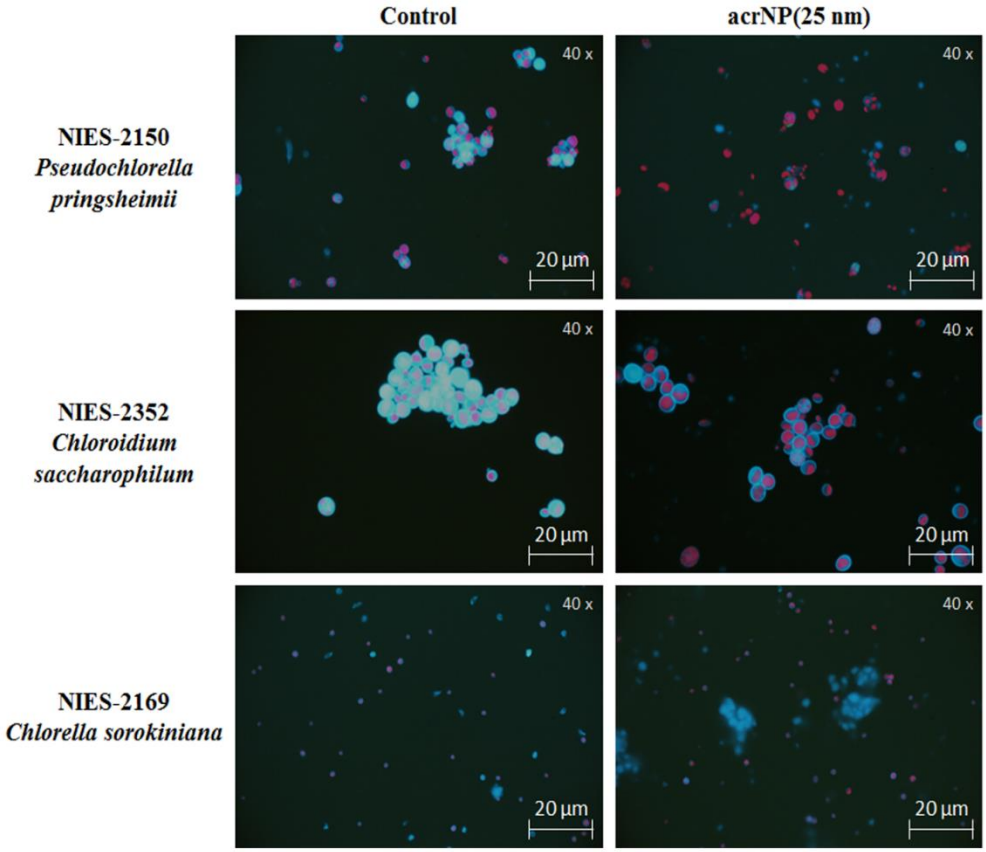

Fig. 3.5 Detection of protoplasts/spheroplasts in *Pseudochlorella pringsheimii*, *Chloroidium saccharophilum*, and *Chlorella sorokiniana* after exposure with isobutyl-cyanoacrylate nanoparticles (acrNPs) (25 nm) for 4 h at a concentration of 1 g/L. Coincubations with Tris-acetate-phosphate containing dispersant but with no nanoparticles NPs were prepared as controls (left lane).

Current study reported that silver nanoparticles, that synthesized from *Bacillus subtilis*, successfully disrupted the cell wall of *Chlorella vulgaris*. The cell wall damage was suggested by the strong adsorption of nanoparticles on the surface of *C. vulgaris* cells that lead to form the "pits/holes" and cause the releasing of intracellular molecules. The cell wall damage due to silver nanoparticles was confirmed by lactate dehydrogenase assay and visually by SEM analysis [12].

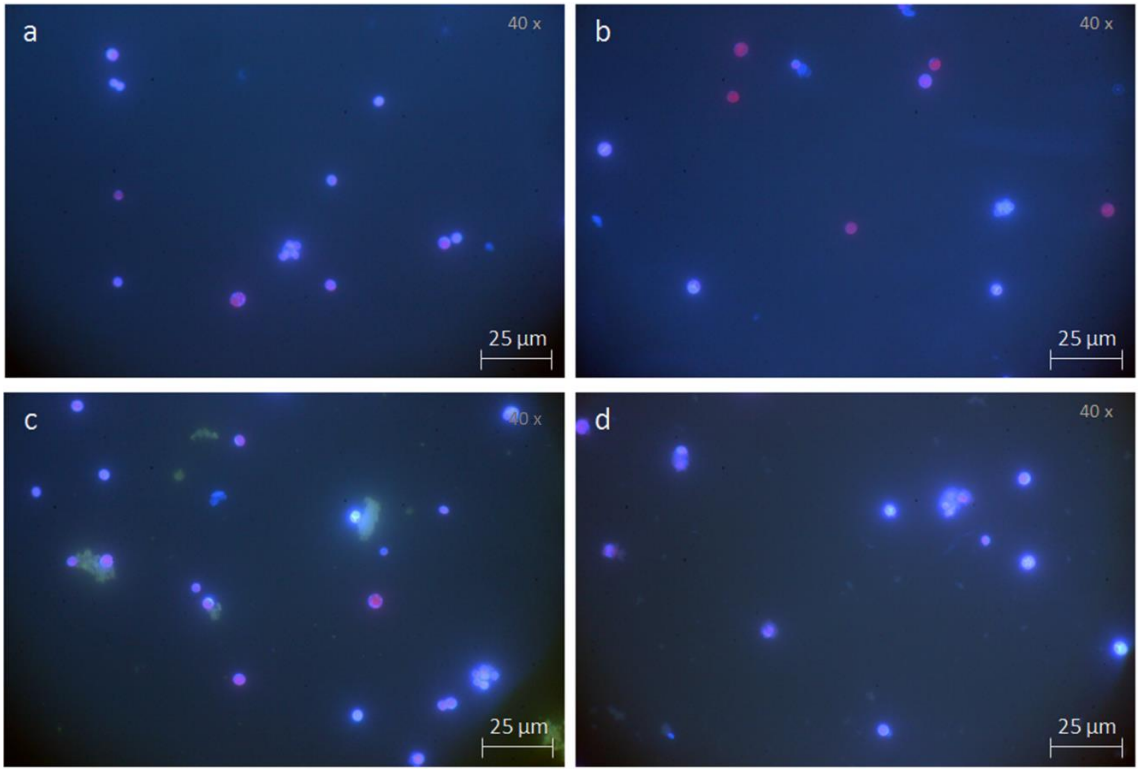

Fig. 3.6 Fluorescence microscopy images of *Chlorella vulgaris* after a 4-h exposure with isobutyl-cyanoacrylate nanoparticles (acrNPs) (180 nm) and nano-sized metal oxides. After the exposure, cell walls were stained with Fluorescent Brightener 28, preceding the microscopic observations. Cells were incubated in TAP medium containing the dispersant used to prepare acrNP(180 nm), as a control (a). Cells were incubated with acrNPs(180 nm) (b), nano-sized ZnO (c), and nano-sized TiO_2 (d). The concentration of acrNPs and nano-sized metal oxides was 1 g • L^{-1}.

One of the prominent attributes of acrNPs, compared with metal oxide nanoparticles, is that they rarely form large aggregates (homo-aggregate), irrespective of particle sizes, whereas metal oxide nanoparticles form aggregates very easily (Fig. 3.7). We suppose repeated collisions of acrNPs with cells could serve as mechanical stress or could be accompanied by a loss in enzyme activity on the cell walls that are secreted for nutrient acquisition [13], resulting in various physiological abnormalities, such as abnormal secretion of the cell-wall hydrolytic enzyme(s). Therefore, acrNPs also may be useful as a new type of stress inducer, substituting for the typical stressors used in research, such as starvation, high temperature, and osmotic pressure. Exposure

of acrNPs to algal cells should be considered as a new method for promoting the production of variable secondary metabolites such as astaxanthin in *Heterococcus* sp.

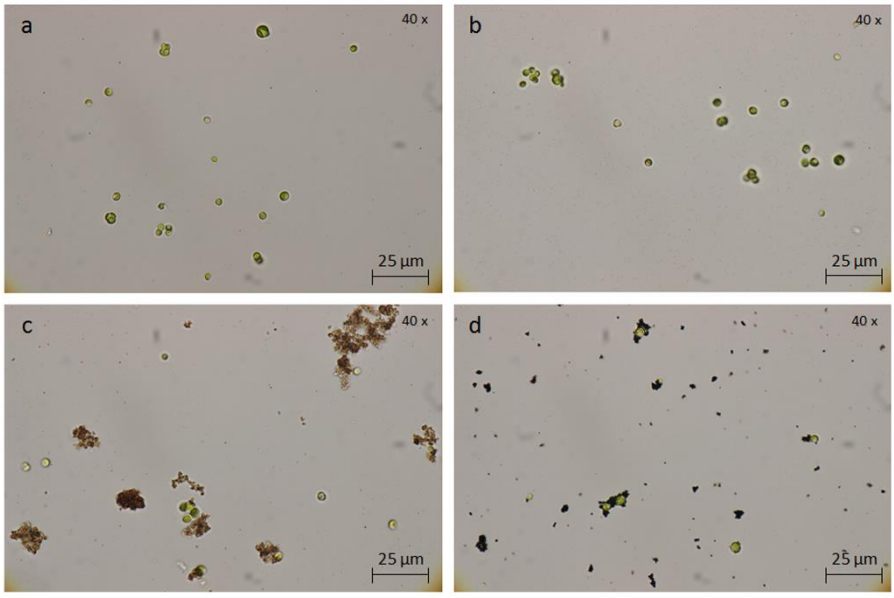

Fig. 3.7 Formation of small agglomerates after a 4-h exposure of *Chlorella vulgaris* with isobutyl-cyanoacrylate nanoparticles (acrNPs) and nano-sized metal oxides. Exposure with no nanoparticles as a control in dispersant-containing Tris-acetate-phosphate medium (a). Results of a 4-h coincubation with acrNPs(180 nm) (1 g/L) (b), nano-sized ZnO (1 g/L) (c), and nano-sized TiO_2 (1 g/L) (d).

3.4 References

1. Tomita Y, Rikimaru-Kaneko A, Hashiguchi K, and Shirotake S. Effect of anionic and cationic n-butylcyanoacrylate nanoparticles on NO and cytokine production in Raw264.7 cells. Immunopharmacology Immunotoxicology. 2011. 33: 730-737.
2. Shirotake S. A new cyanoacrylate colloidal polymer with novel antibacterial mechanism and its application to infection control. Journal of Nanomedicine and Biotherapeutic Discovery. 2014. 4(1): 1-7.
3. Darienko T, Gustavs L, Mudimu O, Menendez CR, Schumann R, Karsten U,

Friedl T, and Proschold T. *Chloroidium*, a common terrestrial coccoid green alga previously assigned to *Chlorella* (Trebouxiophyceae, Chlorophyta). European Journal of Phycology. 2010. 45(1): 79-95.

4. Gorman DS, and Levine RP. Cytochrome f and plastocyanin: their sequence in the photosynthetic electron transport chain of *Chlamydomonas reinhardi*. Proceeding National Academy of Science USA. 1965. 54(6): 1665-1669.
5. Gerken HG, Donohoe B, and Knoshaug EP. Enzymatic cell wall degradation of *Chlorella vulgaris* and other microalgae for biofuels production. Planta. 2013. 237(1): 239-253.
6. Yamada T, and Sakaguchi K. Comparative studies on *Chlorella* cell walls: induction of protoplast formation. Archives of Microbiology. 1982. 132(1): 10-13.
7. Hatano S, Joh T, Miyamoto T, and Yoshimoto M. Preparation of protoplast from *Chlorella ellipsoidea* C-27. Plant Cell Physiology. 1992. 33(5): 651-655.
8. Yamamoto M, Fujishita M, Hirata A, and Kawano S. Regeneration and maturation of daughter cell walls in the autospore-forming green alga *Chlorella vulgaris* (Chlorophyta, Trebouxiphyceae). Journal of Plant Research. 2004. 117: 257-264.
9. Honjoh K, Suga K, Shinohara F, Maruyama I, Miyamoto T, Hatano S, and Iio M. Preparation of Protoplast from *Chlorella vulgaris* K-73122 and cell wall regeneration of protoplast from *C. vulgaris* K-73122 and C-27. Journal of the Faculty of Agriculture Kyushu University. 2003. 47(2): 257-266
10. He X, Dai J, and Wu Q. Identification of sporopollenin as the outer layer of cell wall in microalga *Chlorella protothecoides*. Frontiers in Microbiology. 2016. 7: 1047

11. Ma S, Zhou K, Yang K, and Lin D. Heteroagglomeration of oxide nanoparticles with algal cells: effects of particle type, ionic strength, and pH. Environmental Science and Technology. 2015. 49(2): 932-939.
12. Razack SA, Duraiarasan S, and Mani V. Biosynthesis of silver nanoparticle and its application in cell wall disruption to release carbohydrate and lipid from *C. vulgaris* for biofuel production. Biotechnology reports. 2016. 11:70-76.
13. Sinsabaugh RL, Repert D, Weiland T, Golladay SW, and Linkins AE. Exoenzyme accumulation in epilithic biofilms. Hydrobiologia. 1991. 222: 29-37.

ACKNOWLEDGEMENT

I would like to present this dissertation as the sincere appreciation to all special person who challenged, supported, and kindly encouraged me along the way to finish my doctoral study.

Foremost, I want to offer this endeavor to our **GOD Almighty** for the wisdom he bestowed upon me, the strength, the peace of my mind, and the good health in order to finish this research.

I would like to express my special gratitude and thank to my advisor, **Prof. Takeshi Ohama**, which sincerely and tirelessly helped me in completion of my study. He is the most kind-hearted person that taught me a lot in my study and daily life in Japan. I appreciate all his contributions of energetic enthusiasm, thoughtful ideas, motivation, and generously supports to make my doctoral study experience productive, enjoyable, and memorable. I am also thankful for the excellent example he has provided as a successful Professor and researcher.

I would like to thank my dear **Family (Mama, papa, kak Didik, and Kak Astrid)**, for their love, patience, encouragement, and fully support. For my dear **Pondra Buana**, thank you for always by my side.

My thanks and appreciation also go to **Ohama lab member**. I am especially grateful for **Dr. Tomohito Yamasaki** to help and assist me in solving some experimental problem. I am cherish for time spent with **Dr. Sari Dewi Kurniasih**, for her willingness to help me

not only in research but also in my daily activities. Thank you for being my older sister in Japan. I am thankful to all Bachelor and Master student who make my laboratory time become more enjoyable.

My thanks and appreciation also go to **my Indonesia friends and Thailand friends** for all the great times that we have shared.

Lastly, I am particularly thankful to all faculty member in the school of environmental science and engineering and the members of International Relationship Center (IRC), for their infinite patience and concern with me.

ACHIEVEMENT

List of publications

- Kurniasih, S. D., Yamasaki, T., Kong, F., Okada, S., **Widyaningrum, D**., & Ohama, T. (2016). UV-mediated *Chlamydomonas* mutants with enhanced nuclear transgene expression by disruption of DNA-methylation dependent and independent silencing system . *Plant Molecular Biology, 92*(6), 629-641.

International conferences

- The 5th International Symposium of Frontier Technology (ISFT) (2015, Kunming, China, **Oral**).

Patent

- 特願 (patent application)：JP, 2017-082277

  発明者 (Inventor)： 飯田 大介, 大濱 武, ドゥイヤンタリ ウィディヤンニンルン

  発明の名称：微細藻類増殖抑制剤および微細藻類の増殖を抑制する方法